A Lego® Brewster Angle Microscope for Quantitative Monolayer Film Analysis

Nicholas Benz*

Department of Chemistry, California Polytechnic State University, San Luis Obispo, California 93407

July 3, 2015

Abstract: In order to study single-molecule thick films and their phase behavior we built a Brewster Angle Microscope (BAM). BAM's are inherently expensive due to their accuracy and precision. We built a fully functional BAM using Lego® Mindstorm® kits for the fraction of the price of a commercial BAM. And by utilizing the 10µm patented Lego® tolerance, comparable accuracy was attained. The BAM was mounted to a Langmuir-trough and will be used for laboratory experiments for optics and physical chemistry along with research on lung surfactant and on liquid crystals.

Introduction:

Understanding the morphology of single-molecule thick films can afford valuable knowledge that may forward the world of biophysics and surface chemistry and their many disciplines such as pharmaceuticals, food-coatings, and liquid-crystals.

Langmuir troughs are frequently used to study the isothermic properties of monolayers at the air-water interface. They prove exceptionally useful with the study of phospholipids and proteins. **Figure 1**[1] can be useful to visualizing how one works.

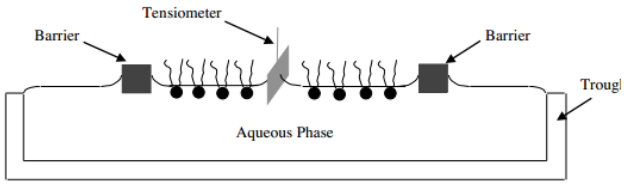

Figure 1: *Profile view of a non-Blodgett Langmuir-trough including a lipid monolayer and an aqueous subphase.*

Upon dispensing a small amount of the sample (diluted in a volatile such as chloroform) onto the insoluble, inert, medium the monolayer quickly disperses across the entire trough area **A**. After a few minutes the volatile solvent is completely evaporated, and a single molecule thick lipid monolayer remains on top of the media. Phospholipids are a popular molecule for film studies due to their ampiphillic behavior. Because of this, nanopure water acts as a perfect subphase for creating a monolayer with the lipid.

Ampiphiles are described as having both hydrophobic and hydrophilic properties. In the case of phospholipids, a hydrophilic head and a hydrophobic tail allow for a bilayer at the air-water interface. As the barrier plates of the trough move inwards, the monolayer is squeezed together, increasing surface pressure **π**. Surface pressure is the difference between the surface tension of a clean interface, γ_{pure}, and the surface tension of the interface with a monolayer, γ_{mono}, as seen in **Equation 1**[1] below.

$$\pi = \gamma_{pure} - \gamma_{mono} \qquad \textbf{[Equation 1]}$$

The Wilhelmy plate detects this change and – with the help of interfacial software- can graph the isothermic compression of surface pressure **π** over trough area **A**. The increasing surface pressure promotes intermolecular interactions between the individual molecules in the monolayer; and depending on the molecular structure and the temperature a multitude of outcomes are possible [1]. **Figure 2**[1] is the basic phosphatidylcholine structure; a positive amine and a negative phosphate make up phosphatidylcholine's zwitterionic head group[1]. Saturation, branching, and length of the "R"

hydrocarbon side chains will drastically influence the surface chemistry of the monolayer upon compression and expansion.

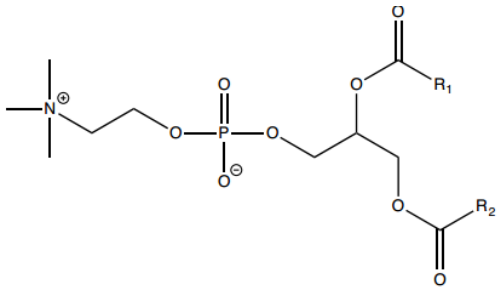

Figure 2: *Phosphatidylcholine parent structure with "R" chains.*

If enough thermal energy is available upon compression then the monolayer can experience a phase shift from a liquid expanded (LE) state to a liquid condensed state (LC)[1]. This phase shift will occur at the transition surface pressure $\boldsymbol{\pi_\tau}$. The trough area difference between the LC and LE states is identified by ΔA. **Figure 3**[1] illustrates these values on a π/A isotherm of a monolayer at different temperatures.

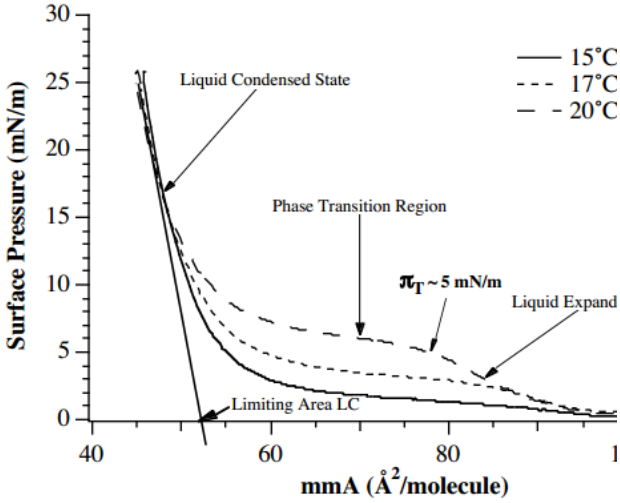

Figure 3: *π/A isotherm with phase denotations and transition pressure.*

With these values and **Equation 2**, a manipulation of the Clapeyron equation[1], the molar latent heat of transition, $\mathbf{Q_m}$, can be found:

$$\frac{d\pi_T}{dT} = \frac{Q_m}{T\Delta A_m} \qquad \textbf{[Equation 2]}$$

Where $\mathbf{d\pi_\tau/dT}$ is the change in transition surface pressure π_τ with respect to temperature T (in degrees Kelvin) and $\mathbf{\Delta A_m}$ is the change in the area of the Langmuir trough occupied by the monolayer[1]. Due to the fact that the experiment occurs under isothermic conditions, $\mathbf{Q_m}$ is equal to enthalpy, $\mathbf{H_m}$[1]. Using Qm and the following equation, the molar entropy of the layer, $\mathbf{\Delta S_m}$, can be found:

$$Q_m = T\Delta S_m \qquad \textbf{[Equation 3]}^{1}$$

The entropy of the system will be directly related to the state that it is in. More tightly packed and organized LC states equate to a lower overall entropy. This allows for predictions to be made about lipids based on their structure. Typically, longer, more saturated fatty acid tails exhibit tighter packing opposed to unsaturated and branched fatty acid chains. This causes saturated lipids to have an increased surface activity which relates to a lower surface tension whereas unsaturated lipids experience a higher surface tension due to their smaller surface activity.

When examining the isothermic phase behavior of proteins, there are deviations from lipid behavior but the theory behind Langmuir monolayers still applies. Protein (and lipid) film analysis is compounded by inquiries regarding the kinetics behind adsorption and reabsorption of the films during compressions and expansions. This is primarily governed by electrostatic forces, steric interactions, and London Dispersion Forces (LDF) which are solely contingent on the structure of the protein[2-4]. **Figure 4**[5] illustrates two common states a colloid solution (in this case a protein) may be found in.

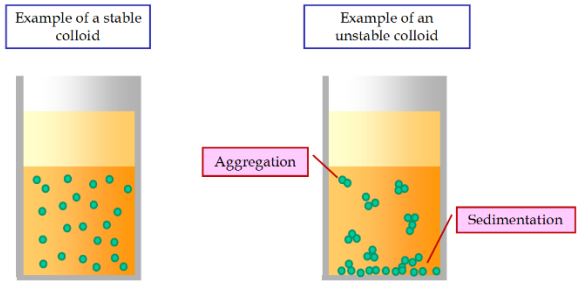

Figure 4: *Comparison of colloid stability.*

Upon compression the protein may experience cross-linking, stacking, and aggregation which may prevent a uniform interfacial adsorbtion of the protein[6]. Explaining such phenomena, when they occur, is a prominent aspect of colloid film chemistry.

Lung Surfactant:

There are many compounds in nature that behave as monolayer films, mainly biomembranes, one of which is Lung Surfactant (LS). Lung surfactant is a complex mixture primarily consisting of dipalmitophosphatidylcholine (DPPC), palmitic acid, and surfactant proteins A, B, C, and D[7-8]. While other non-negligible lipids as well as cholesterol are also present, LS research is primarily concerned with the aforementioned compounds. Lung Surfactant benefits from being very surface active – a characteristic allowing it to maintain very low surface tension and very high surface pressure- and having fast readsorption rates at the air-water interface [8]. Coupled, these characteristics help LS decrease the surface tension of the interior of the lungs down to zero[8]. This is remarkable considering that without LS, the human body would need to devote a majority of it metabolic capacity to expanding and compressing the lungs[8]. Unfortunately, some people are afflicted by a lung disease that results in inactivated lung surfactant. Acute Respiratory Distress Syndrome (ARDS) is accountable for 150,000 American cases a year with a 40% mortality rate[9-13]. Due to the monolayer behavior of LS and its large fractional composition of DPPC lung surfactant can be studied on Langmuir-troughs and, as will be discussed shortly, studied via Brewster Angle Microscopy. Both of these analytical techniques have provided clarity to how both proper and improper LS function at a molecular level.

Ultimately, a proper compression-expansion isotherm of a monolayer can acquire tremendous data of the polymorphism for a lipid or a protein –as it mimics the respiratory cycle found in the human pulmonary system. This information is enhanced by the thermodynamic data calculated and makes it possible to quantify any postulations or trends.

While thermodynamic and isothermal data are insightful, this experimentation generously benefits from measuring the surface density of the monolayer too. Once compressed, the film may undergo many variant states such as aggregation, cross-linking, and stacking to form multilayers. As a multilayer, the film will experience an exchange between molecules at the surface and molecules in the subphase [8]. And in the case of LS, the blood protein Albumin may displace the surfactant and diffuse to the surface layer. This is the case in ARDS patients who may have Albumin concentrations in their LS above a "safe" threshold [8]. The existence of multilayered surface creates for an exchange that is even more difficult to model than a monolayer; the top layer is the only portion to influence the surface-pressure and may appear as a monolayer but will behave entirely differently. Understanding the kinetics behind this exchange undoubtedly helps to understand more about ARDS.

Upon expansion, the monolayer must readsorb on top of the subphase. Ideally, the monolayer will completely adsorb to the surface and will have a uniform surface density. Unfortunately

this does not always occur; surfactant can remain in sub-surface aggregates or even aggregate at the surface itself, compromising the performance of the surfactant as surface-tension reducer [8].

Revealing the phase-morphology and film-behavior of a complex mixture such as lung surfactant along with the globular proteins it interacts with, Albumin, is of major concern for physical chemists and biophysicists. Accordingly, this inquiry begs for an instrumental method for measuring surface density in addition to isothermal and thermodynamic data.

Quantitative Brewster Angle Microscopy:

While several techniques have been developed for measuring surface density, they are inherently limited in their own various ways. Fluorescent light microscopy (FLM), scanning force microscopy (SFM), and scanning near-field optical microscopy (SNOM) are restricted by details such as solubility, artifacts, fluorescent probes, and working with single component monolayers[14-16].

With the integration and manipulation of Brewster's Law, however, a very effective method for determining the surface density of monolayer films has been constructed. Brewster's Law spawned off of the theory that at a specific angle, θ_p, incoming polarized light striking a dielectric surface would only reflect partially. Polarized light normal to the plane of incidence –and accordingly parallel to the surface- will reflect off of the surface while the light component parallel to the plane of incidence will not[17]. **Figure 5**[17] illustrates how Brewster's angle works.

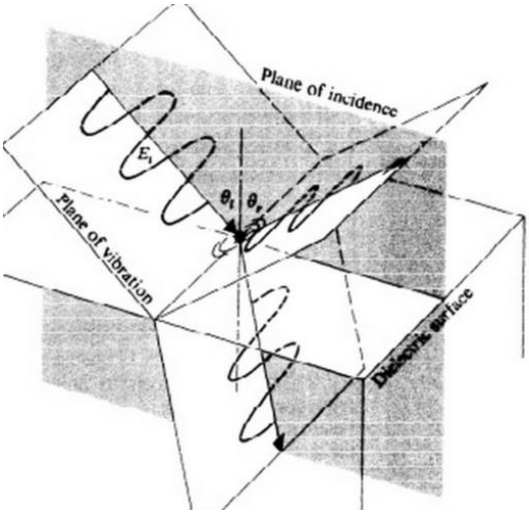

Figure 5: *A polarized incident light wave reflecting at the Brewster angle of a dielectric surface.*

The s-polarized light (perpendicular to the surface) along with a remainder of the p-polarized light are then transmitted through the surface. The incident angle and transmitted angle are complementary angles, so they can be appropriately arranged to make:

$$\theta_t = 90° - \theta_P$$

and can be inserted into **Equation 4**, **Snell's Law**:

$$n_i sin\theta_p = n_t sin\theta_t \qquad \textbf{[Equation 4]}$$

to make:

$$n_i sin\theta_p = n_t cos\theta_p$$

And by simple trigonometric functions **Equation 5**, **Brewster's Law,** is found:

$$tan\theta_p = \frac{n_t}{n_i} \qquad \textbf{[Equation 5]}$$

Here, n_t is the refractive index for the surface, such as water or glass (n_t=1.5 and n_t=1.33, respectively). And n_i is the refractive index of air (n_i=1). When observing a surface at its Brewster angle with polarized light, the surface will appear to be black, seemingly vacant of any reflected light[17].

With the addition of a single molecule thick film, however, there is a third refractive index, n_{film}, at play. Due to the fact that each substance has its own unique refractive index, the added film will not have the same Brewster Angle as the surface it is added to. The film will be able to reflect some of the incident light –for a 2nm thick monolayer film, $R=10^{-6}$ roughly[8]. This reflectivity, **R**, is related to the refractive index, $\mathbf{n_{film}}$, and is used to solve for the surface density, **Γ.** This is the essence of Brewster Angle Microscopy (BAM).

Reflectivity can be calculated using **Equation 6**, a combination of both **Snell's Law** and the **Fresnel** equations (**Equation 7**) formulated by **Winsel** *et al*[17-20].

$$R = \frac{I_r}{I_0} = (\frac{\propto - n_w}{\propto + n_w})^2 \qquad \textbf{[Equation 6]}$$

$$R = R_{\parallel} = R_{\perp} = (\frac{n_t - n_i}{n_t + n_i})^2 \qquad \textbf{[Equation 7]}$$

In **Equation 6**, I_r and I_0 represent the reflected and incident light intensity, respectively while n_w is the refractive index of the subphase. The variable α is a simplification of **Snell's Law** as can be seen in **Equation 8**:

$$\alpha = \frac{cos\theta_t}{cos\theta_i} \qquad \textbf{[Equation 8]}$$

Without knowing the exact value of θ_t, it is easier to manipulate **Equation 8** so that only θ_i is required for the calculation. Beginning with **Snell's Law**, n_i can be ignored since $n_i=1$ for air:

$$\frac{sin\theta_i}{n_t} = cos\theta_t$$

Then, by applying the Pythagorean trigonometric identity:

$$cos\theta_t = \sqrt{1 - (\frac{sin\theta_i}{n_w})^2}$$

Lastly, this can then be substituted for $\cos(\theta_t)$ in **Equation 8** to make **Equation 9:**

$$\alpha = \frac{cos\theta_t}{cos\theta_i} = \frac{\sqrt{1-(\frac{sin\theta_i}{n_w})^2}}{cos\theta_i} \qquad \textbf{[Equation 9]}$$

In ultimatum, the angle of the incident beam θ_i is used to find α which in turn is used to determine the reflectivity, R. With this data, a calibration curve can be made plotting the grayscale **G** against reflectivity **R**. The grayscale is a measured brightness of the film using a charge-coupled device (CCD) camera.

Plotting grayscale against θ_i will produce the exact Brewster angle; occurring at the minimum of the parabolic distribution. Using the reflectivity calibration curve, grayscale values can be related to reflectivity values. If the reflectivity **R** is known then thickness of the film **d** or the exact refractive index of the film $\mathbf{n_{film}}$ can be determined using **Equation 10**[18-21]**.**

$$R = (\pi \frac{d}{\lambda}) \frac{(n_{film}^2 - n_w^2 - 1 + \frac{n_w^2}{n_{film}^2})^2}{1 + n_w^2} \qquad \textbf{[Equation 10]}$$

New variables in this equation include **d** and **λ** or the thickness of the film in nanometers and the wavelength of the light source in nanometers, respectively. This equation must be satisfied by the approximation that $d<<\lambda$[8]**.**

Calculating the surface concentration, or surface density Γ is of the main benefits of BAM. And it can be determined using **Equation 11**, a homologation of the Fersnel equations and Maxwell-Garnett theory.

$$\frac{n_{film}^2 - n_w^2}{n_{film}^2 + 2n_w^2} = \frac{\Gamma}{\Gamma_{cryst}} \frac{n_{cryst}^2 - n_w^2}{n_{cryst}^2 + 2n_w^2} \qquad \textbf{[Equation 11]}$$

In **Equation 11**, n_{fillm} is the refractive index of the film deposited, n_w is the refractive index of the subphase, and n_{cryst} is the refractive index of the film as a crystallized solid. Likewise, Γ is the surface density of the film and Γ_{cryst} is the surface density of the crystallized film. This is exceptionally useful for substances with documented crystalline characteristics[8]. Additionally, the work of Frey *et al* maintained

that the refractive index of the film was linearly proportional to the surface density of the film[8].

A Novel Application of BAM:

As discussed earlier, BAM is a useful tool in research regarding human lung surfactant. Through an effective collaboration Dr. Jonathan G. Fernsler and Dr. Joseph A. Zasadzinski published their research in this specific field. "Competitive Adsorption: A Physical Model for Lung Surfactant Inactivation" reports their findings on the adsorption and desorption characteristics of both surfactant molecules and of albumin during isothermic compressions and expansions. By comparing the surface density Γ of the substances against trough area, surface pressure, and concentration they were able to build a theoretical model explaining how lung surfactant inactivation may occur at a molecular level. This model lays the groundwork for ongoing and future research for Acute Respiratory Distress Syndrome.

Brewster Angle Microscopes:

While Brewster Angle Microscopes can be bought commercially they tend to be expensive, mandating price tags that don't fall below $40K for the *entry model* instruments. The microscope apparatus itself only consists of a light source -typically a HeNe or red-diode laser- a detector –typically a CCD camera- and a goniometer to precisely control the angle of the camera and laser. A BAM schematic is shown below in **Figure 6** along with some of the pertinent optical theory[22]**.**

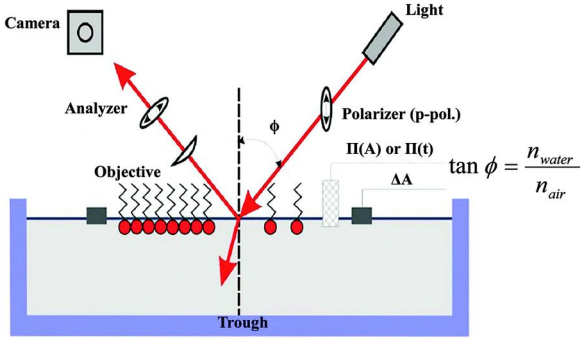

Figure 6: *a simple schematic of BAM. It is imperative that the light is p-polarized upon incidence with the film.*

Although some commercial BAM's come equipped with a Langmuir-trough –a hefty expense in its own- the bulk of the price can be attributed to the goniometer. **Figure 7**[24] shows what a professional BAM from KSV® looks like.

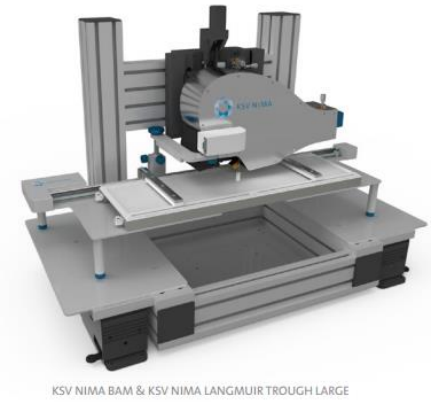

Figure 7: *A KSV® NIMA BAM equipped with a Langmuir-trough.*

At first glance, a goniometer appears to be an overpriced protractor, but it is crucial to the functionality of the BAM. The purpose of the microscope is to be able to observe and experiment on a molecular film that is only ~2nm thick. At this scale, any vibration or movement is beyond noticeable and can compromise the ability to perform quality lab work. Additionally, it may be necessary to sustain a precise angle (even down to the 0.01°) for several hours at a time with zero chance of fluctuation.

An Alternative BAM:

A Biochemistry post-doc was confronted with the same financial stricture as we were and resorted to building a BAM out of a Lego® Mindstorm® kit[23]. Although he blogged about it and was featured in articles, his build-schematic

was never made available. After cursory analysis we deduced that we could build a more effective and more capable BAM for our needs.

The main allure to using Lego® bricks is their patented 10 µm tolerance. While not strictly intended for scientific research, that degree of accuracy is perfectly suitable and was our best bet for constructing a budget BAM. Furthermore, modular design is a virtue in scientific apparatus' that may need to be disassembled and moved; Lego® bricks by nature are extremely modular.

We began the build by constructing two separate "arms," one for the laser and one for the CCD camera. Each arm is powered by a Lego® servo motor that is connected to a gear box; the motors spin in unison. The gear box has a final drive ratio of 1:112.5 allowing us to adjust the angle of the two arms very finely. A third servo motor helps mount the camera to the arm, but it also is utilized as a zoom function by pushing and pulling the camera.

The first build was a success and operated as intended; it can be seen in **Figure 8**.

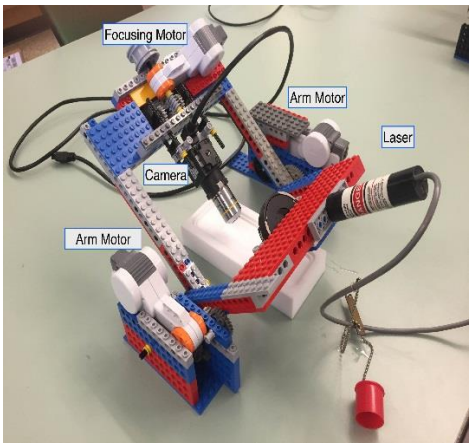

Figure 8: *Protoype build of BAM. Increasing proportions and bolstering its structural integrity were of top concerns for the rebuild.*

The Lego® Mindstorm® kits were sourced from the Cal Poly Physics Department along with a surplus CCD camera, red-diode laser, a 10x microscope objective, and a polarizer. A miniature Teflon® Langmuir-trough was provided by Cal Poly Chemistry Department.

The dimensions of the laser and the CCD camera were compatible with the dimensions of Lego® bricks. This allowed for an extremely convenient build that only required two Lego® pieces to be shaved down slightly in order to properly mount the camera. A second polarizer was cut and inserted inside of the 10x objective lens for the purpose of polarizing any contaminate light ensuring that all light entering the CCD is p-polarized.

After filling the trough with deionized water, the Brewster Angle was found. Next, less than 10µl of 1.006 mg/ml of dipalmitophosphatidylcholine (DPPC) in chloroform was deposited on top of the water subphase using a Hamilton 50 µl gas-tight syringe. A Teflon® barrier block was used to compress the monolayer and we were able to capture the image seen in **Figure 9**

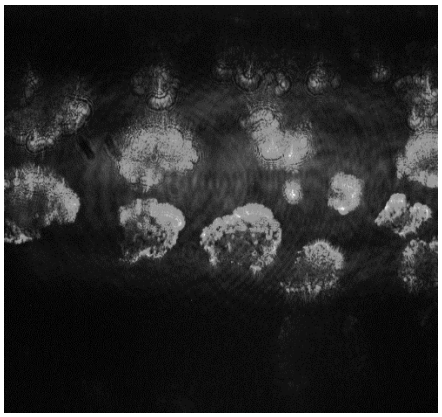

Figure 9: *1.006 mg/ml of DPPC deposited onto deionized water with visible approximate 400 micron wide LC domains.*

The acquisition was a tremendous success and while limited in the field of view it proved to have the potential to be competitive with a commercial-grade instrument. **Figure 10**[25] illustrates a comparison of a DPPC monolayer analyzed by a professional BAM.

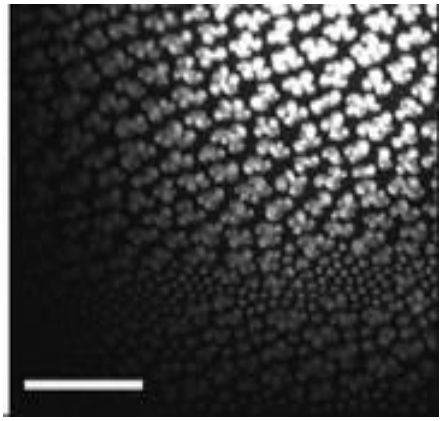

Figure 10: *DPPC monolayer at 7mN/m.*

Despite not being able to measure the surface pressure at that preliminary stage, the accomplishment remains. In both images, bright DPPC liquid-condensed domains can be seen reflecting p-polarized light.

The next step was to revamp the BAM to a fully functioning size so that it may be mounted to a Langmuir-trough in the physical chemistry laboratory.

The entire build write up was documented with pictures and can be read in the Appendix. Major modifications include widening the arms, rebuilding the gear boxes to maximize support and minimize torque, and adding an additional brace to the camera as to minimize any movement or sagging when using the zoom function.

The CCD camera, laser, and polarizer were all sourced from the Physics Department. The camera is a Point Grey® Flea3® FL3-FW-14S3C firewire CCD camera. The laser is a Lasermax Inc.® red-diode laser. And the polarizer is a Thor Labs Inc.® rotatable polarizer.

Lego® Mindstorm® kits come equipped with an NXT® control module capable of running the servo motors in a stepwise fashion. The module operates through a LabVIEW® script and can run new programs that are written in LabVIEW®. In order to utilize the full capability of the motors and NXT® controller, a new program was written.

Originally, the program was intended to run both arm-motors synchronously (rather than one-at-a-time as it does out of the box) and to throttle the power output of the motors, both within an easy-to-use control panel. But we discovered that the CCD could be controlled by a lightweight open-source camera acquisition program, ImageJ®. Conveniently, ImageJ® is compatible with LabVIEW® and could integrated into the same script for the motor-controller. As the program sits now, it is capable of still-shot and video acquisition, grayscale reading, and focus stacking –a powerful feature that negates any shortcomings of a small field of view by stitching together multiple successive frames into one high resolution image. The program also includes a scale bar on the output screen, a necessity with micro-scale lab work.

Results:

Only a few experiments were run on the rebuilt BAM, but were enough to assert that it was capable and effective with higher-performance than the previous iteration. A grayscale distribution was made to calculate where the exact Brewster angle was for our Bam. And a grayscale-Reflectivity calibration curve was made to compare against a BAM Dr. Jonathan Fernsler used at UCSB using **Equation 9** and **Equation 6**. **Figure 10** and **Figure 11** show the grayscale distribution and the grayscale calibration, respectively.

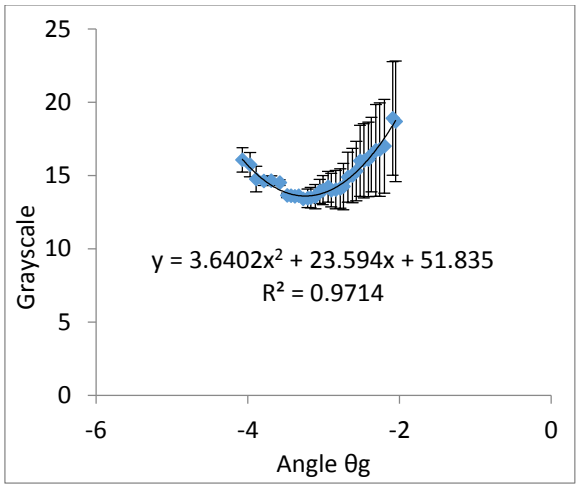

Figure 10: *The grayscale value detected by the CCD verses the angle of the BAM. Θ_g=0 is the Brewster Angle, roughly 53.1°.*

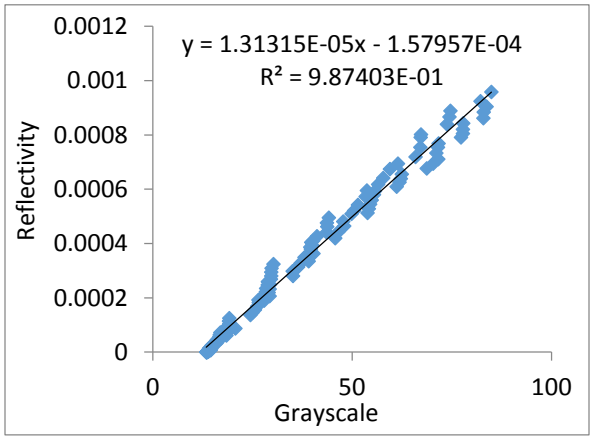

Figure 11: *Calculated Reflectivity verses the Grayscale value at angle Θ_g. A Reflectivity value of 5.39x10^{-8} was acquired at the Brewster Angle.*

The distribution and calibration curve were consistent with Dr. Fernsler's data, although the sensitivity of the image acquisition will be increased for further experimentation. This will be done by decreasing the shutter speed, lowering the frame rate, and also decreasing the resolution of the acquisition. Regardless of future iterations, the prototype performed as expected, thus proving the functionality of this BAM.

Conclusion:

Ultimately, the project was a success. An expensive, high-performance optical instrument was made for less than 2% of its commercial equivalent.

And with the promising grayscale calibration data, the BAM will an excellent instrument for continued research and lab work. This microscope will see use in an optics and physical chemistry experiments. And it will certainly be used for the continuation of Dr. Jonathan Fernsler's lung surfactant research and will see use in liquid crystal experiments as they, too, can behave as films and benefit from analysis of their phase morphology and surface density.

[1] Hagen, Dr. John P. Phopholipid Monolayers. Chemistry 354 Physical Chemistry Lab Manual. Department of Chemistry and Biochemistry. Cal Poly SLO. http://chemweb.calpoly.edu/jhagen/Phospholipid.pdf.

[2] Derjaguin, B.V.; Landau, L. *Acta Physiochim*. URSS **1941**. 14, 633-662.

[3] Verwey, E.J.W.; Overbeek, J.T.G. *Theory of the Stability of Lyophobi Colloids*; Elsevier: Amsterdam, **1948**.

[4] Russel, W.B.; Saville, D.A.; Schowalter, W.R. *Colloidal Dispersions;* Cambridge University Press: Cambridge, U.K., 1989.

[5] Colloid. Wikipedia. May 28, **2015**. https://en.wikipedia.org/wiki/Colloid. Accessed June 2015.

[6] Murray, Brent S.; Cattin, Benoit; Schuler, Elke; Sonmez, Zahlia O. Response of Adsorbed Protein Films to Rapid Expansion. Food Colloids Group, Procter Department of Food Science, University of Leeds, Leeds UK. Langmuir 2002. American Chemical Society. November 2, **2002**. http://pubs.acs.org/doi/pdf/10.1021/la026050u. Accessed June 2015.

[7] Bernhard, W.; Mottaghian, J.; Gebert, A.; Rau, G.A.; con der Hardt, H.; Poets, C.F. *Am. J. Respir. Crit. Care Med.* **2000**, 162(4), 1524-1533.

[8] Fernsler, Jonathan G.; Zasadzinski, Joseph A.; *Competitive Adosprtion: A Physical Model for Lung Surfactant Inactivation*. Langmuir Article. Pubs ACS 2009. June 2009.

[9] Rubenfield, G.D.; Caldwell, E.; Peabody, E.; Weaver, J.; Martin, D.P.; Neff, M.; Stern, E.J.; Hudson, L.D.N. *Engl. J. Med.* **2005**, 353(16), 1685-1693.

[10] Spragg, R.G. Abnormalities of lung surfactant function in patients with acute lung injury. In *Adult Respiratory Distress Syndrome*. Zapol, W.M., Lemaire, F., Eds,; Marcel Dekker: New York, 1991; Vol. 50, pp 381-395.

[11] Schmidt, R.; Markart, P.; Ruppert, C.; Wygrecka, M.; Kuchebuch, T.; Walmarth, D.; Seeger, W.; Guentehr, A. *Respiratory Res.* **2007**, 55.

[12] Raghavendran, K.; Pryhuber, G.S.; Chess, P.R.; Davidson, B.A.; Knight, P.R.; Notter, R.H. *Curr. Med. Chem.* **2008**, 15, 1911-1924.

[13] Dahlem, P.; van Aalderen, W.M.C.; Bos, A.P *Paediatr. Resp. Rev.* **2007**. 8, 348-362.

[14] Galla, HJ; Bourdos, N.; von Nahmen, A.; Amrein, M.; Sieber, M. **1998**. *The role of pulmonary protein C during the breath cycle*. Thin Solid Films 327-329: 632-635.

[15] Honig, D.; Mobius, D. *Direct visualization of monolayers at air-water interface by Brewster Angle Microscopy.* J. Phys Chem. **1991**. 95: 4590-4592.

[16] Discher, B.M.; Schief, W.R.; Vogel, V; Hall, S.B. *Phase separation in monolayers of pulmonary surfactant phospholipids at the air-water interface: composition and structure.* **1991**. Biophys J 77: 2051-2061.

[17] Hecht, Eugene. Optics. Fourth Edition. Pearson Education Inc. Addison Wesley **2002**.

[18] Frey, W.; Schief, W. R.; Vogel, V.; Hall, S.B. *Langmuir* **1996**. 12, 1312-1320.

[19] Winsel, K.; Honig, D.; Lunkenheimer, K.; Geggel, K.; Witt, C. *Euro. Biophys.* J. **2003**. 32, 544-522.

[20] de Mul, M.N.G.; Mann, J.A. *Langmuir* **1998**, 14, 2455-2466.

[21] Azzam, R.M.A.; Bahara, N.M. *Ellipsometry and Polarized Light*. Elsevier, B.V.: Amsterdam, The Netherlands, **1987.**

[22] He, Lin; Lin, Feng; Li, Xingag; Sui, Hong; Xu, Zhenghe. Interfacial science in unconventional petroleum production: from fundamentals to applications. Royal Society of Chemistry. May 19, 2015. http://pubs.rsc.org/en/content/articlelanding/2015/cs/c5cs00102a#!divAbstract. Accessed June 2015.

[23] Mathew. Brewster angle Lego microscope. Errant Science. October 1, 2012. http://errantscience.com/blog/2012/10/01/bam-on-the-cheap/. Accessed June 2015.

[24] KSV NIMA Products: Brewster Angle Microscope. Biolin Scientific. http://www.biolinscientific.com/ksvnima/products/?card=KP6. Accessed June 2015.

[25] Brezesinski, Gerald; Mohwald, Helmuth; Stefaniu, Christina. *Polymer-capped magnetite nanoparticles change the 2D structure of DPPC model membranes*. RSC Pubs.: **2012**.

Appendix: Lego Bam manual

Nicholas Benz, Vincent Nguyen and Jonathan Fernsler

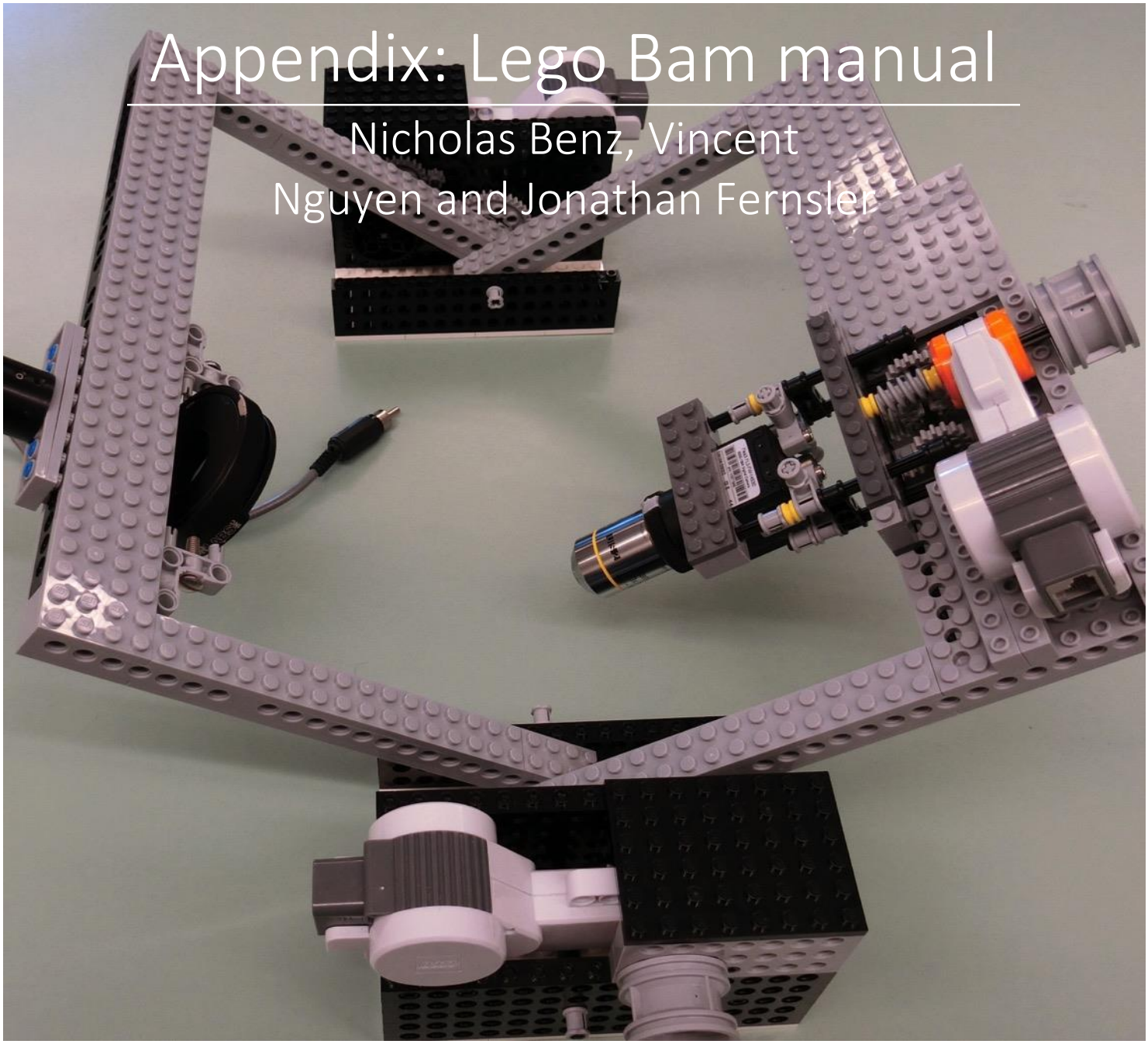

1

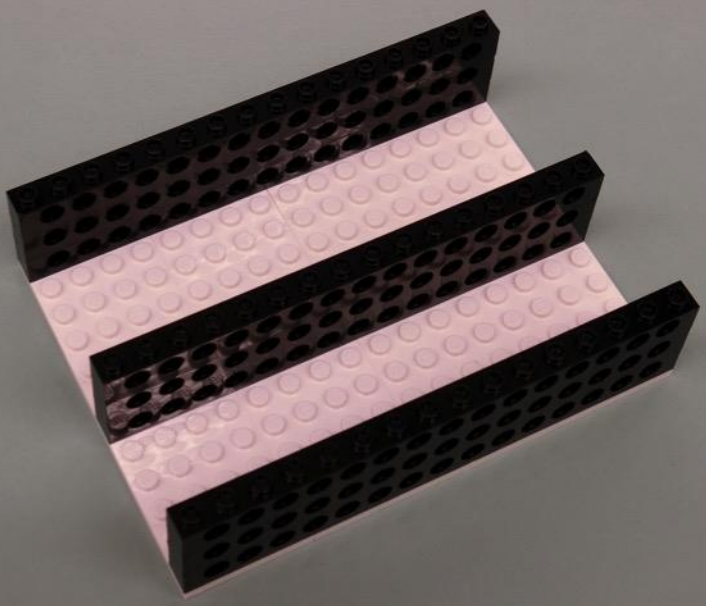

2

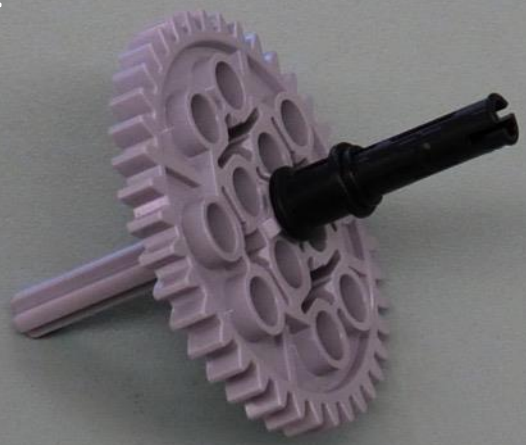

3

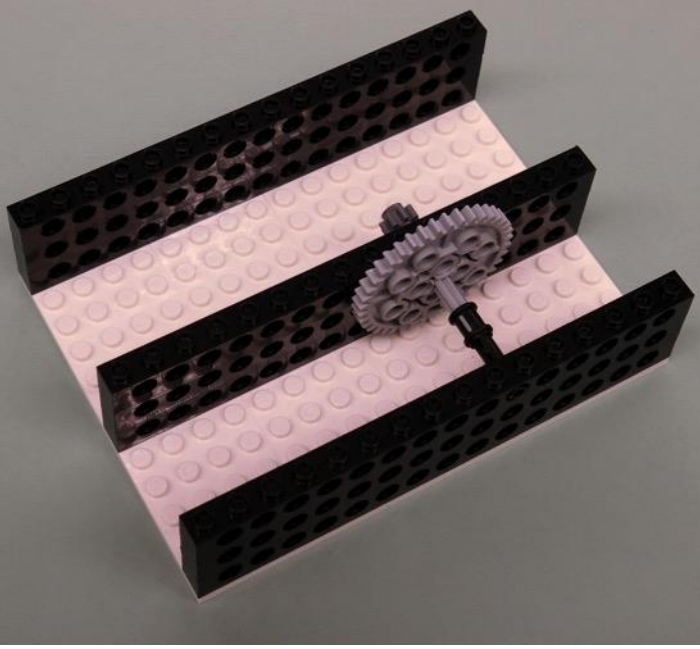

Arm motors

1

Pieces needed:

4x12 white base plates (x2)

1x16 black technic bricks (x9)

2

Pieces needed:

4 long gray rod (x1)

64 tooth gear (x1)

black piece from Minstorm kit (x1)

3

Pieces needed:

12 tooth gear

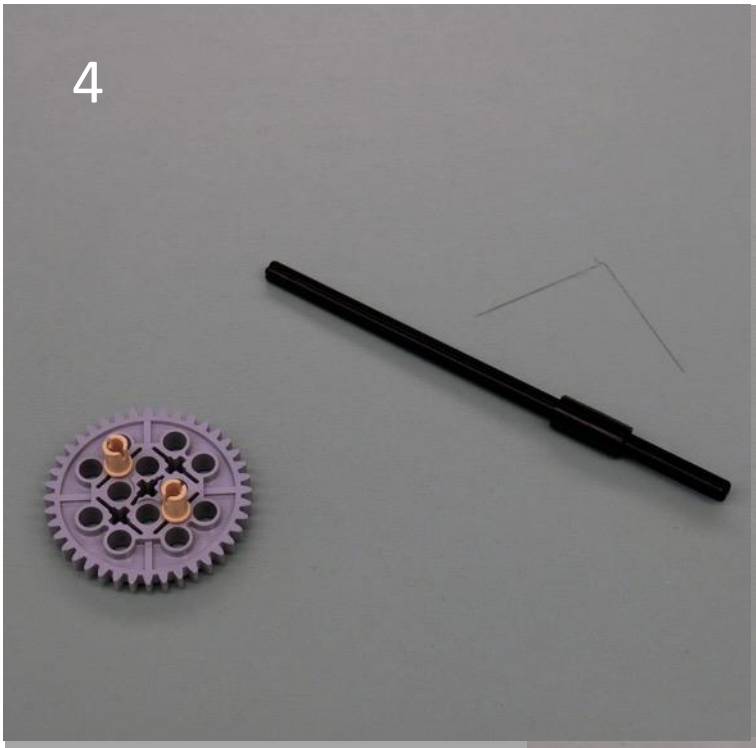

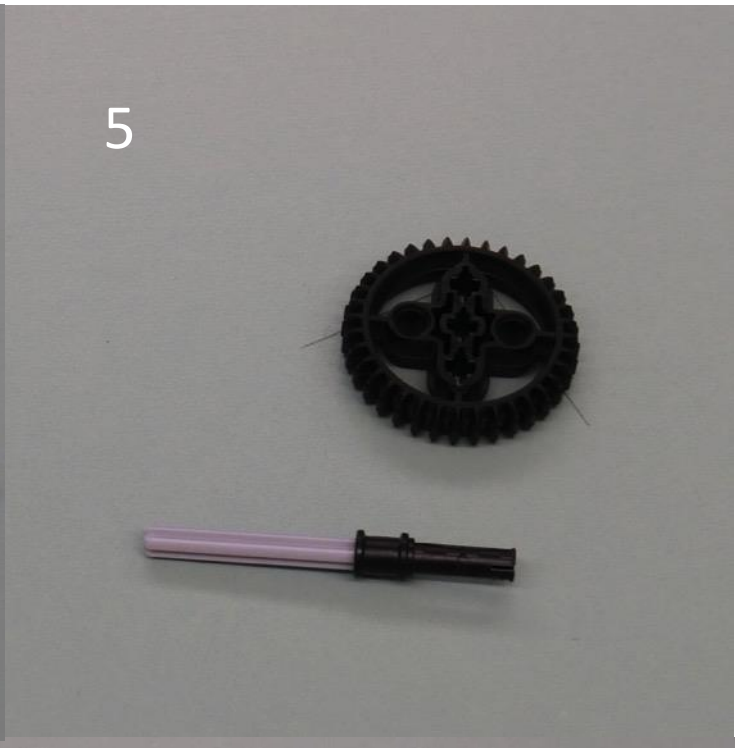

4

Pieces needed:

64 tooth gear

cross/smooth connectors (x2)

12 long rod

4 long rod

rod connector

5

Pieces needed:

4 long gray rod (x1)

64 tooth gear (x1)

black

6

Pieces needed:

12 tooth gear

6 Rotate 180° from previous page

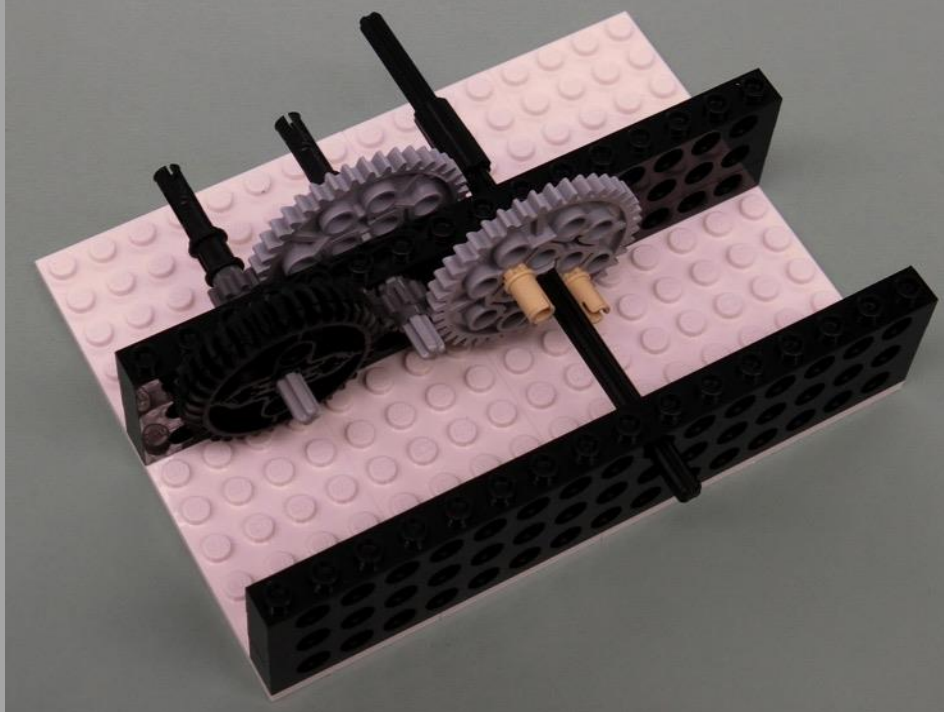

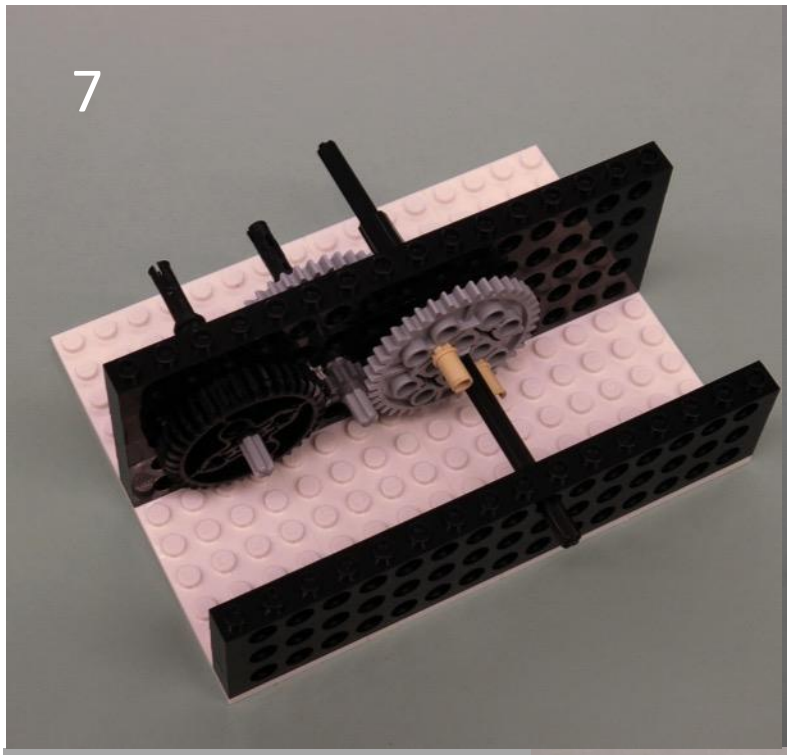

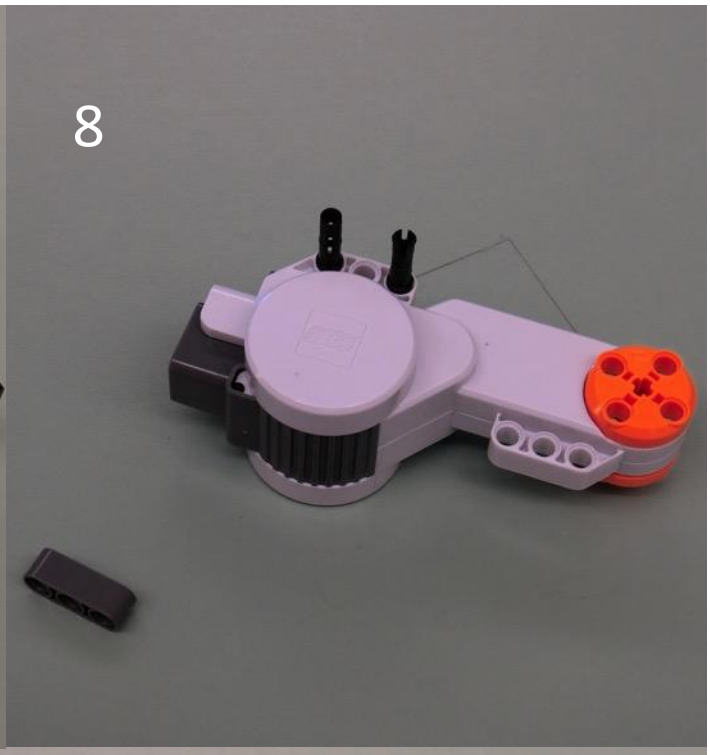

7

Pieces needed:

1x16 black technic bricks

8

Pieces needed:

4 long rounded technic piece

Mindstorm motor

3 long black connector (x2)

9

Click motor into technic bricks as shown

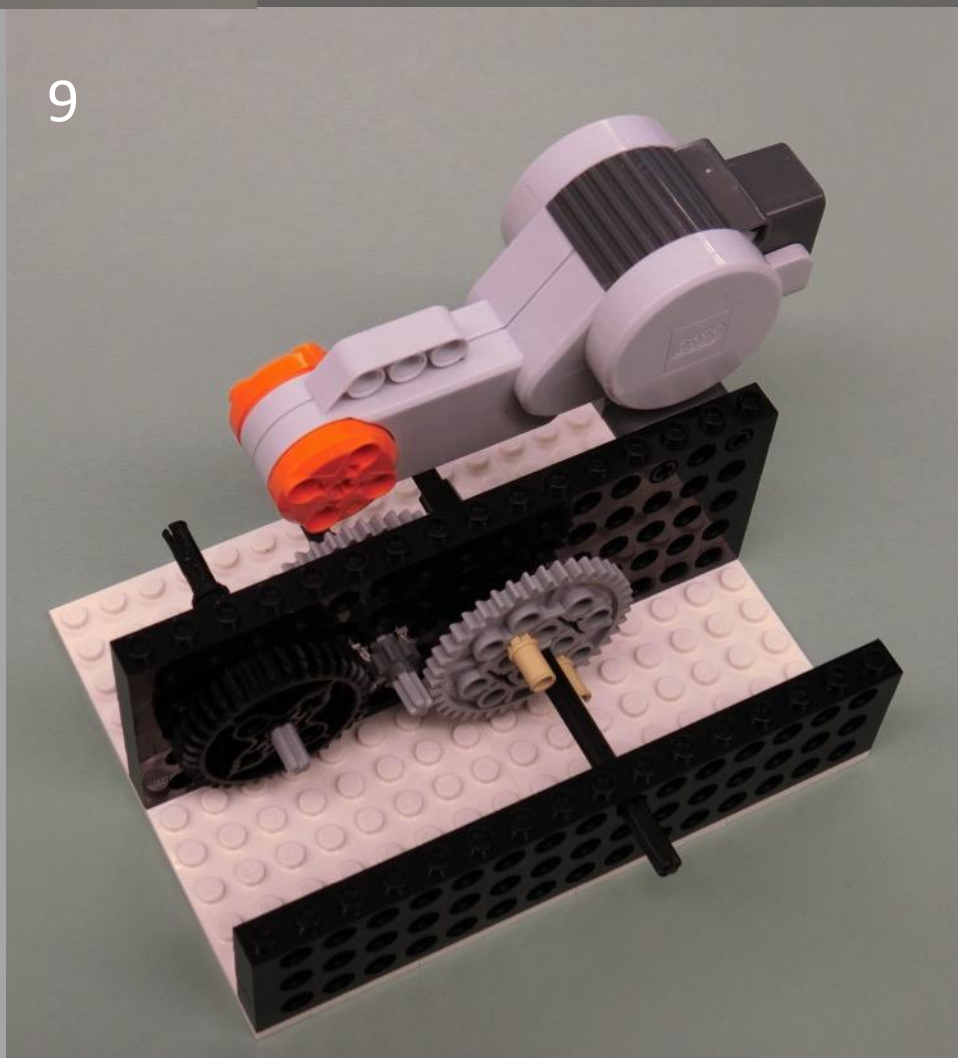

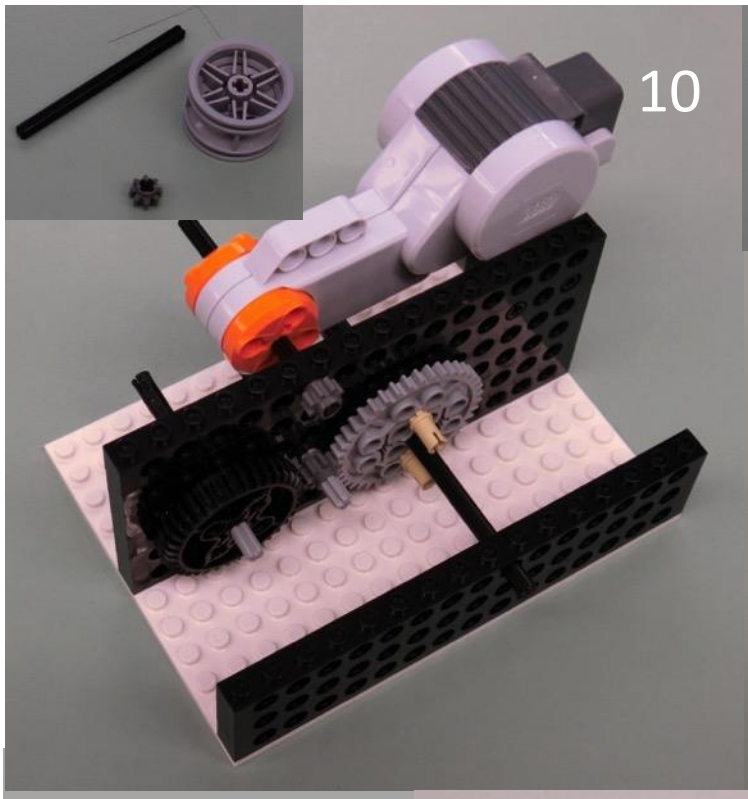

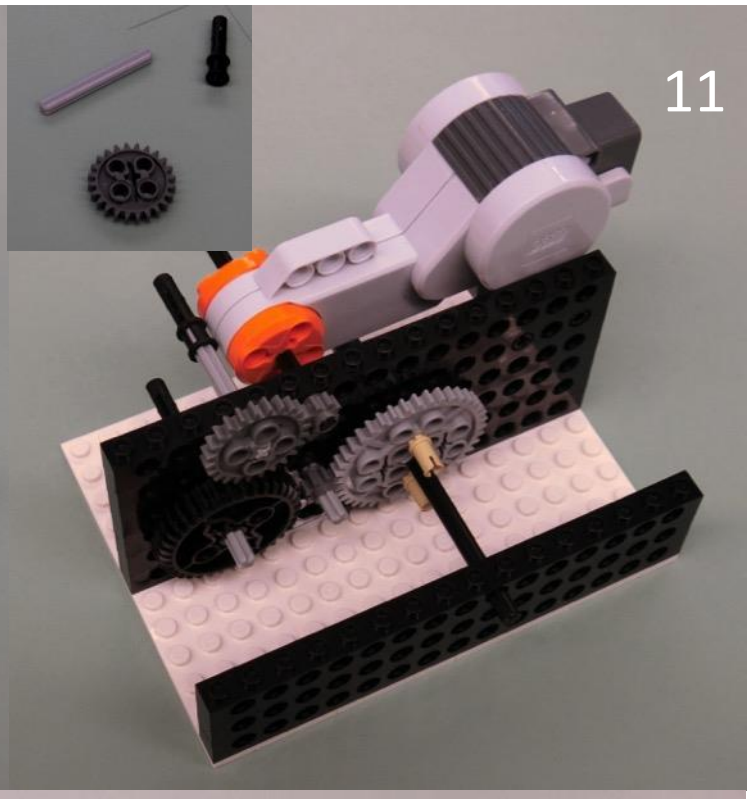

10

Pieces needed:

8 long black rod

12 tooth gear

Mindstorm wheel (can be added to manually turn motor)

11

Pieces needed:

6 long gray rod

3 long black connector

36 tooth gear

12

Pieces needed:

16 long black technic bricks (x2)

2 long black connector (x2)

12 Rotate 180° from previous step

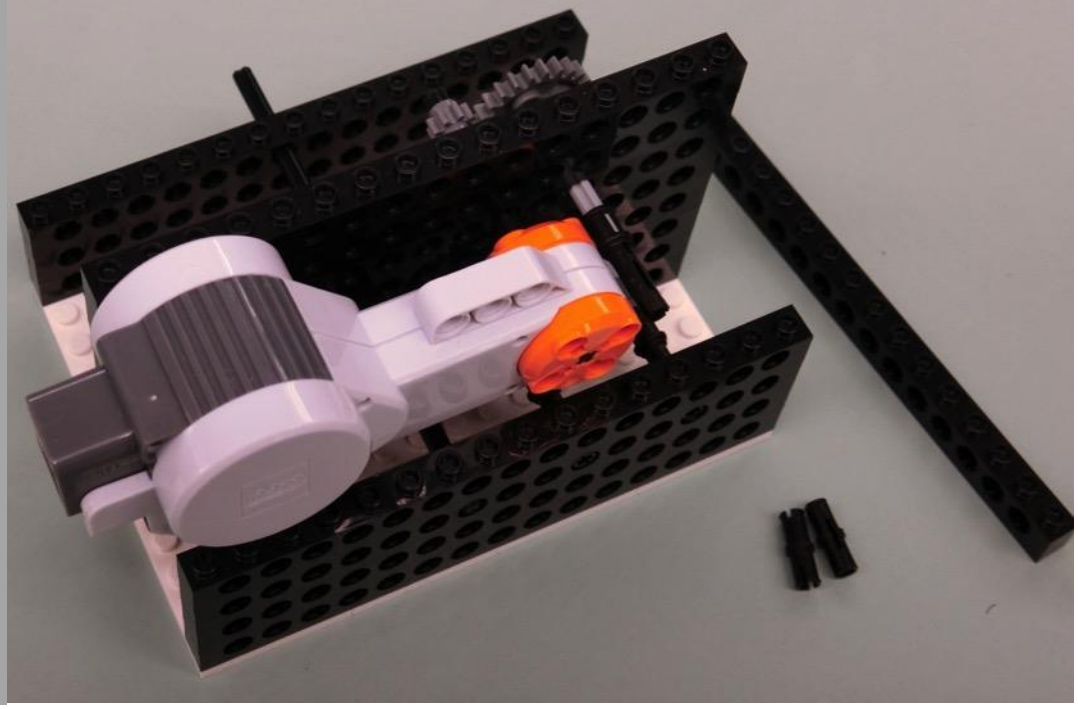

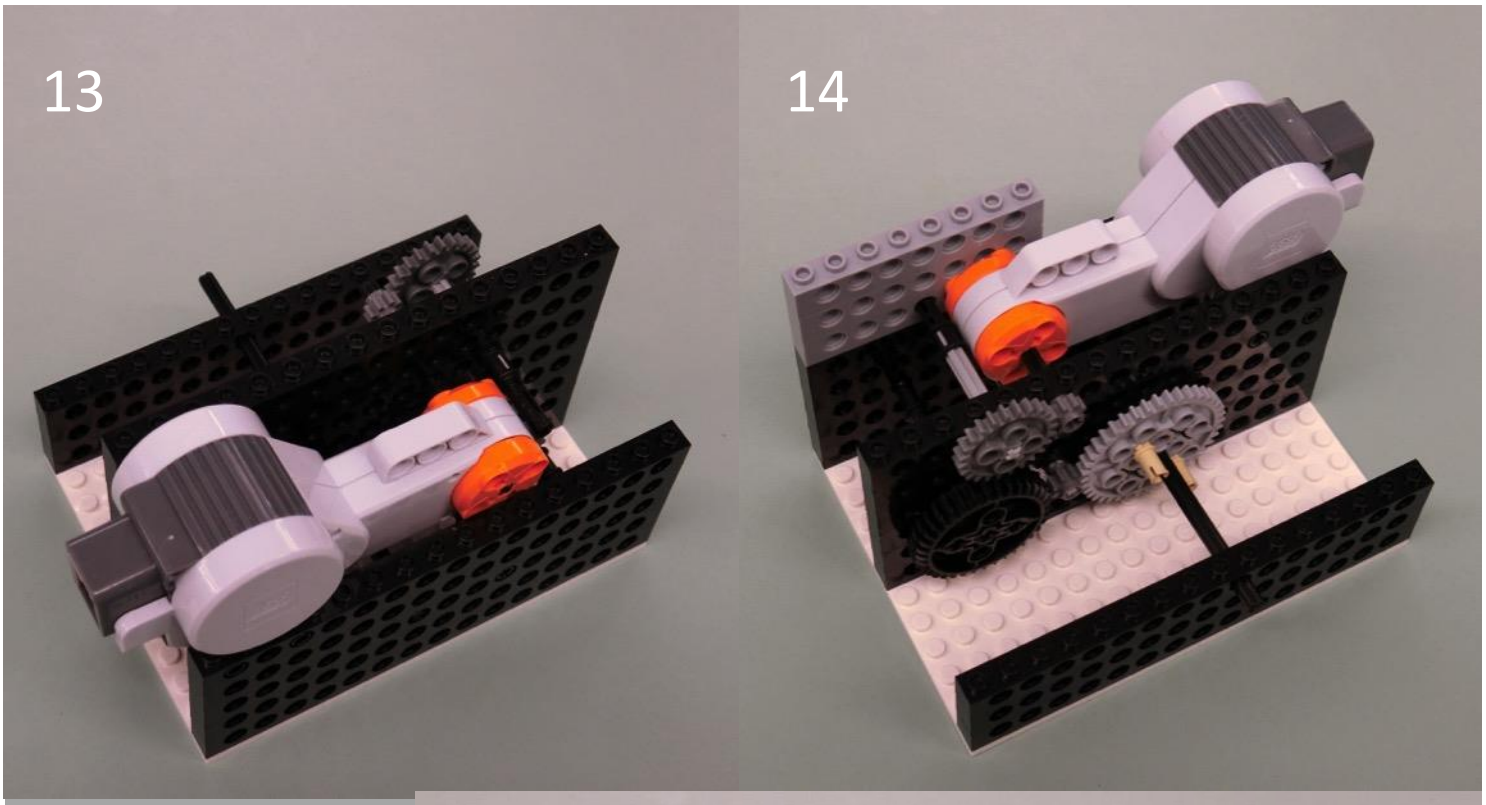

13 Click motor into black technic brick from previous step using connectors

14 Pieces needed:

8 long gray technic brick (x3)

15 Pieces needed:

16 long black technic bricks (x2)
6x8 black plate

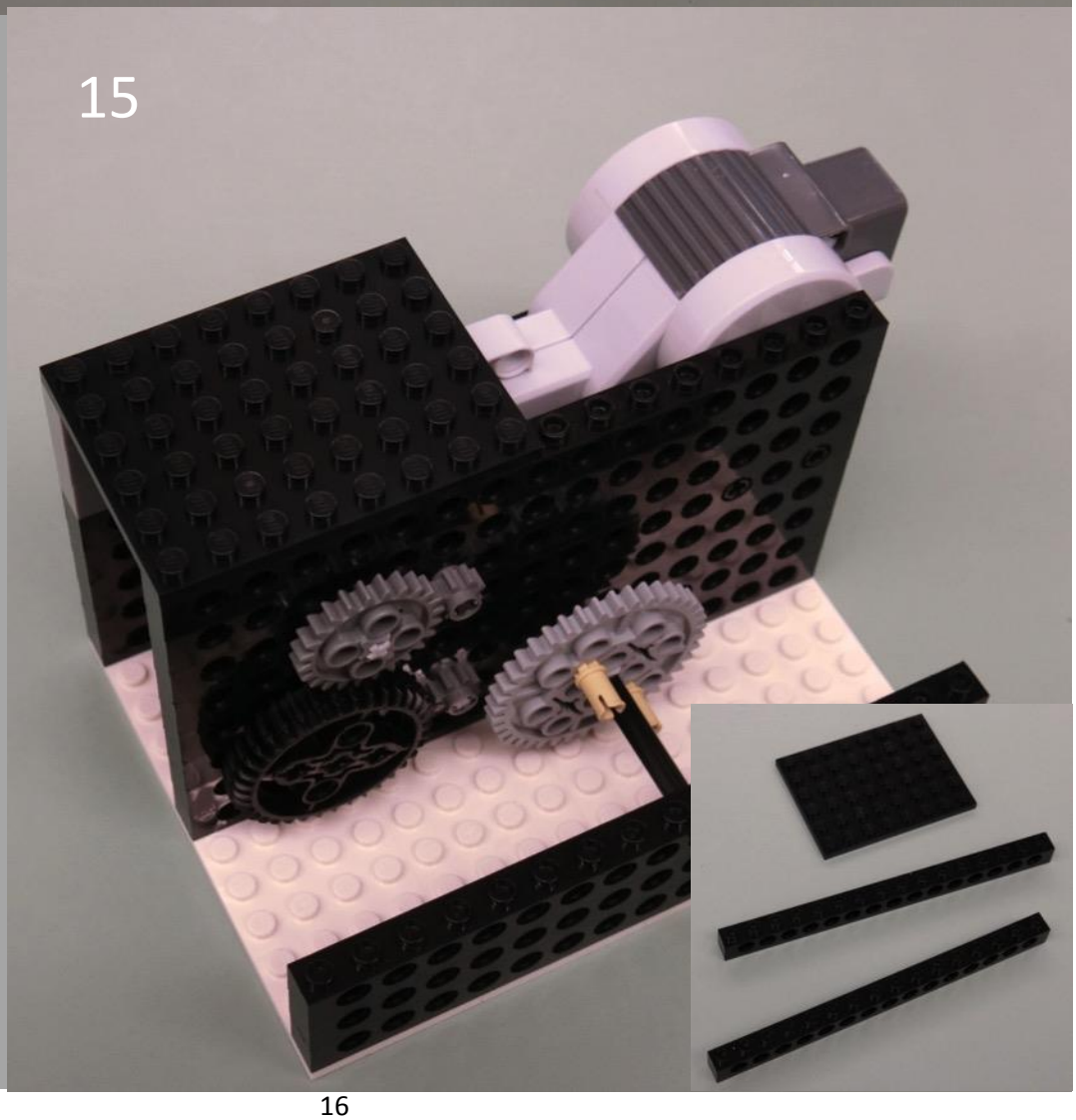

16

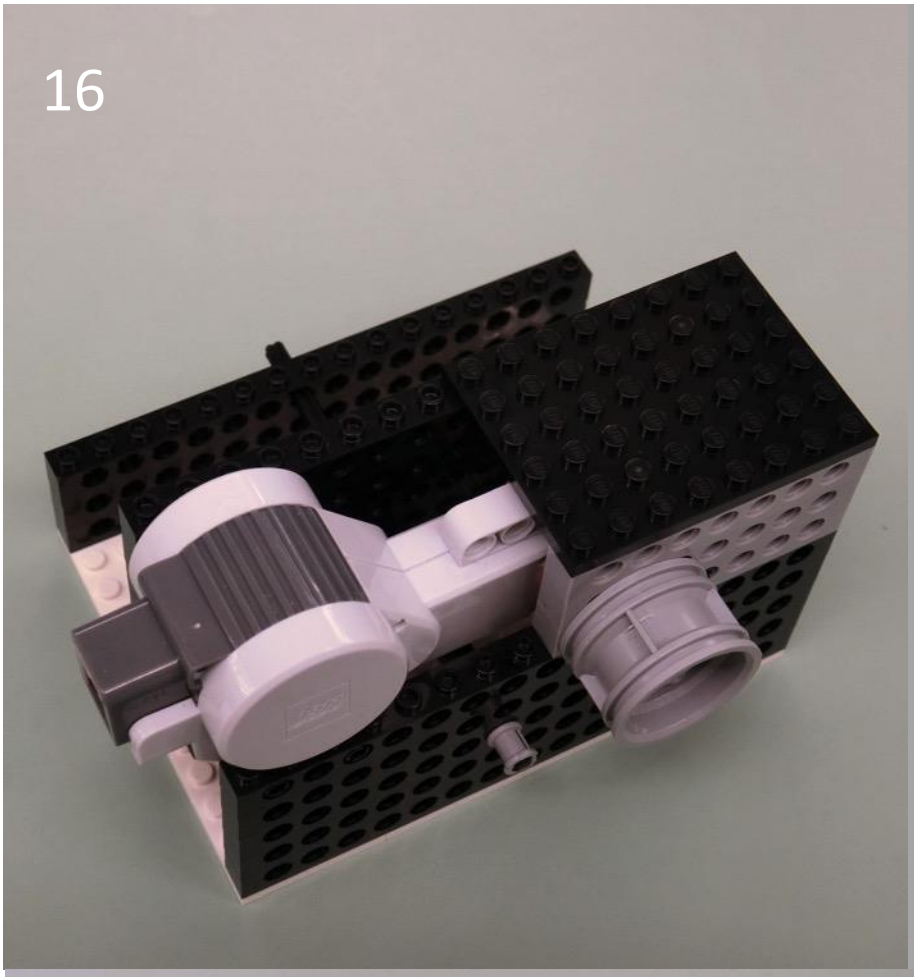

16

Pieces needed:

Wheel (from step 10)

Gray friction fit piece

17

Repeat steps 1-16 to build a second arm motor

17

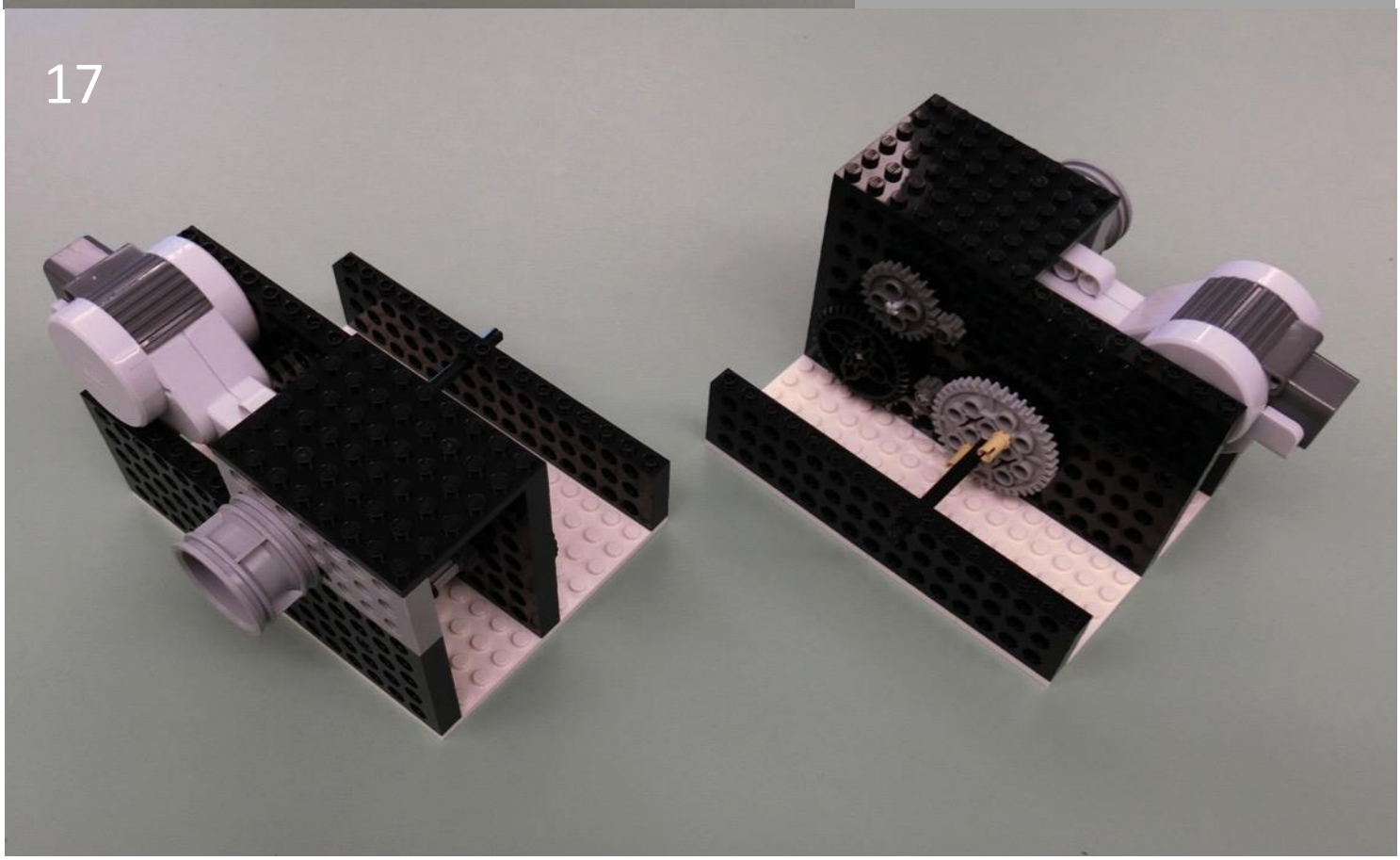

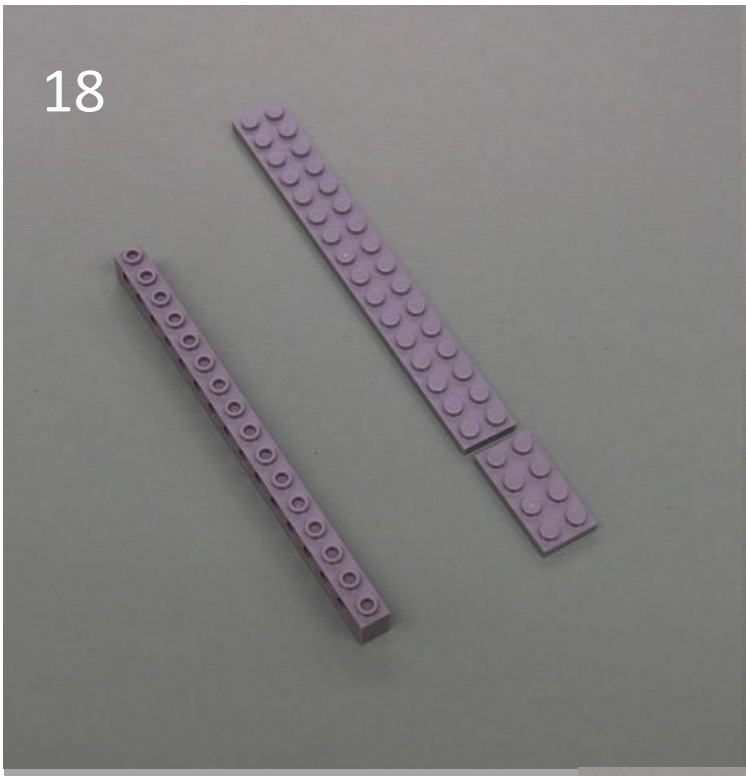

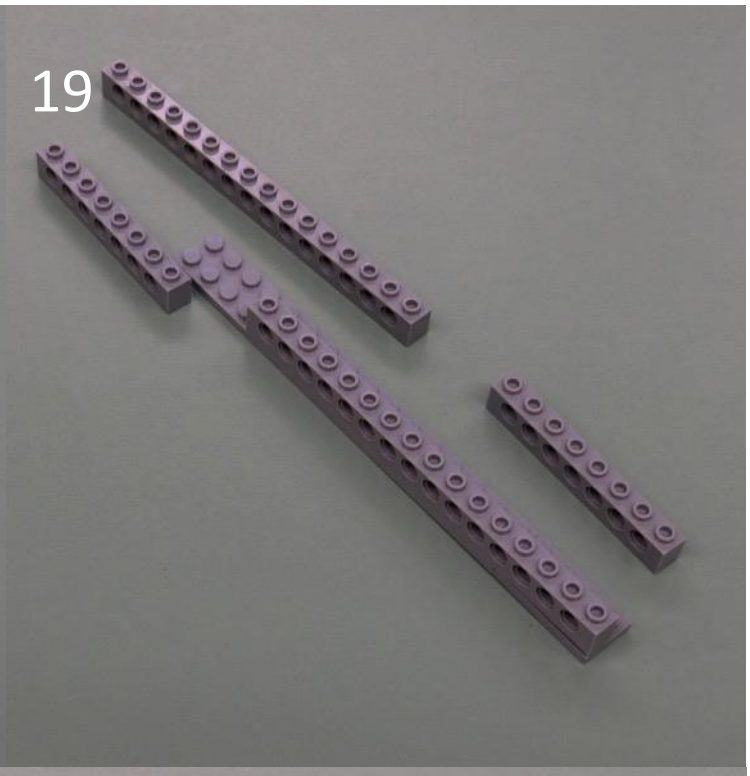

Laser arm

18

Pieces needed:

16 long gray technic brick

2x4 gray plate

2x16 gray plate

19

Pieces needed:

16 long gray technic brick

8 long gray technic brick (x2)

20

Pieces needed:

2x4 gray plate

2x16 gray plate

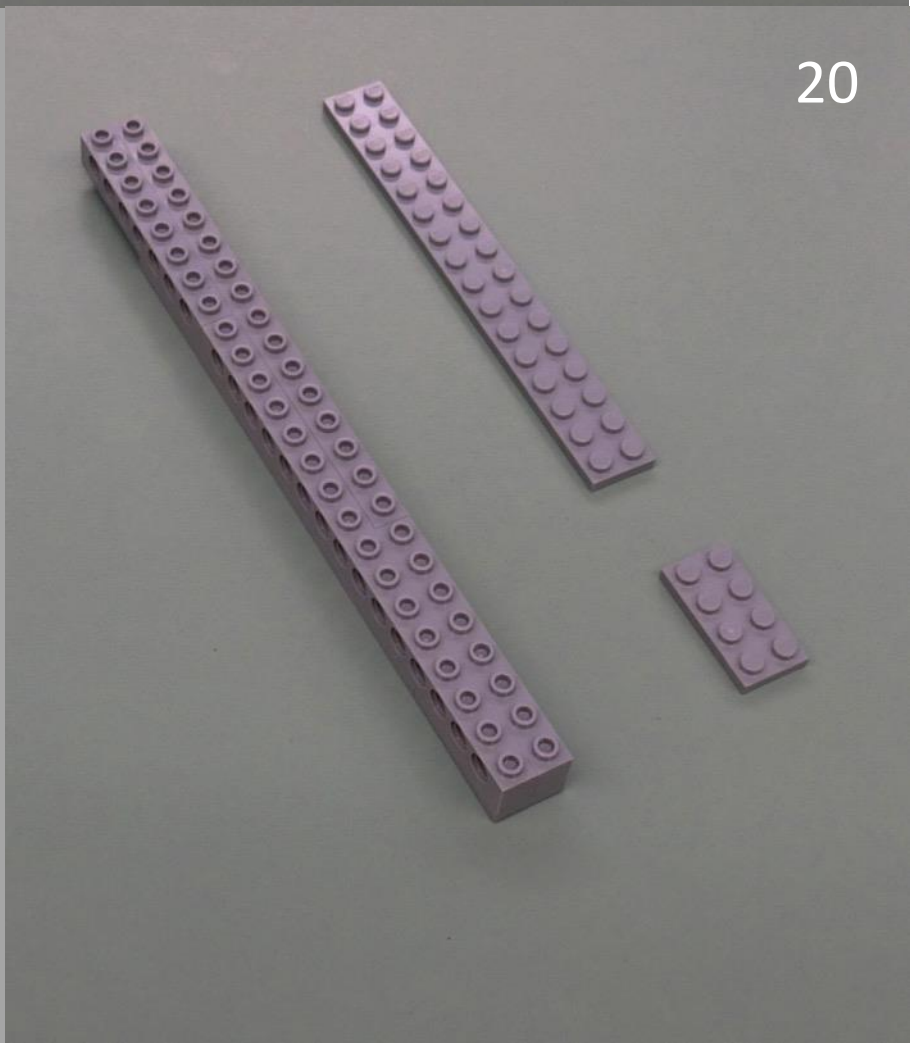

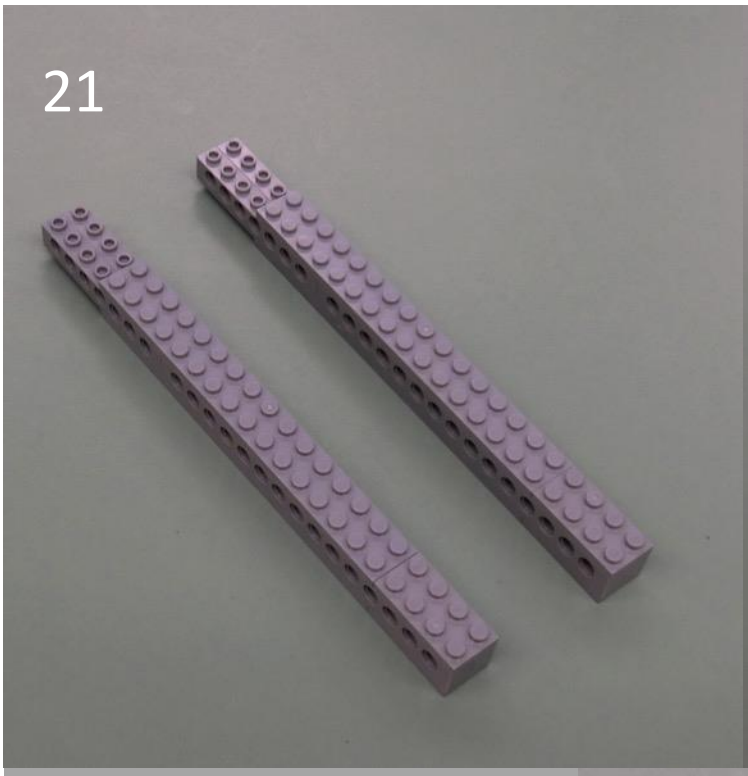

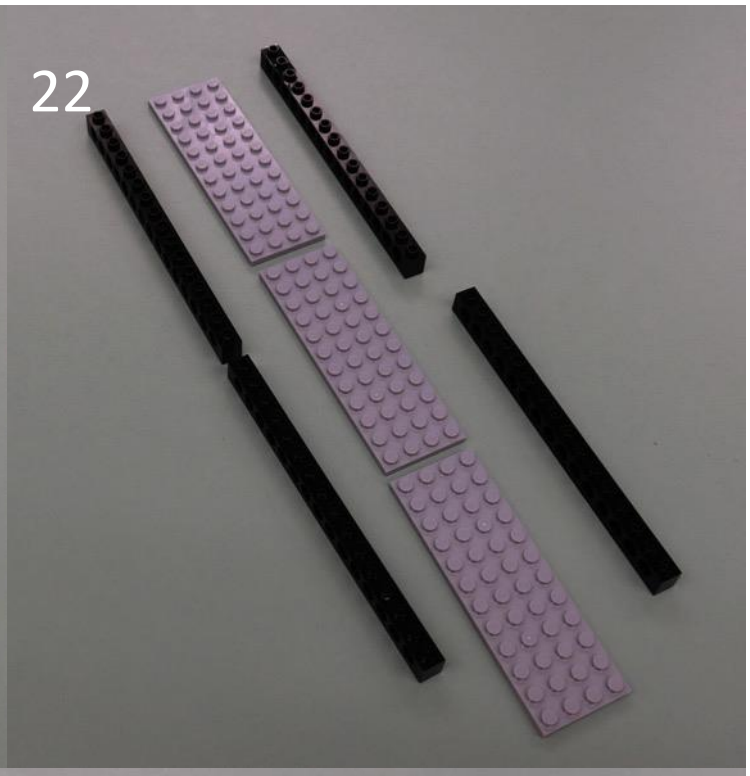

21 Repeat steps18-20 to build second leg

22 Pieces needed:

16 long black technic brick

4x12 gray plate (x3)

23 Pieces needed:

12 long gray technic brick

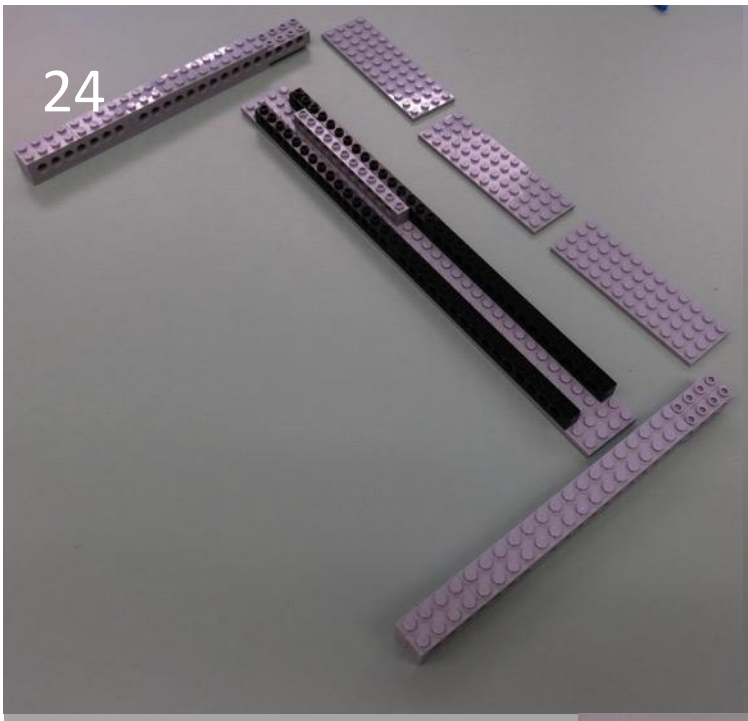

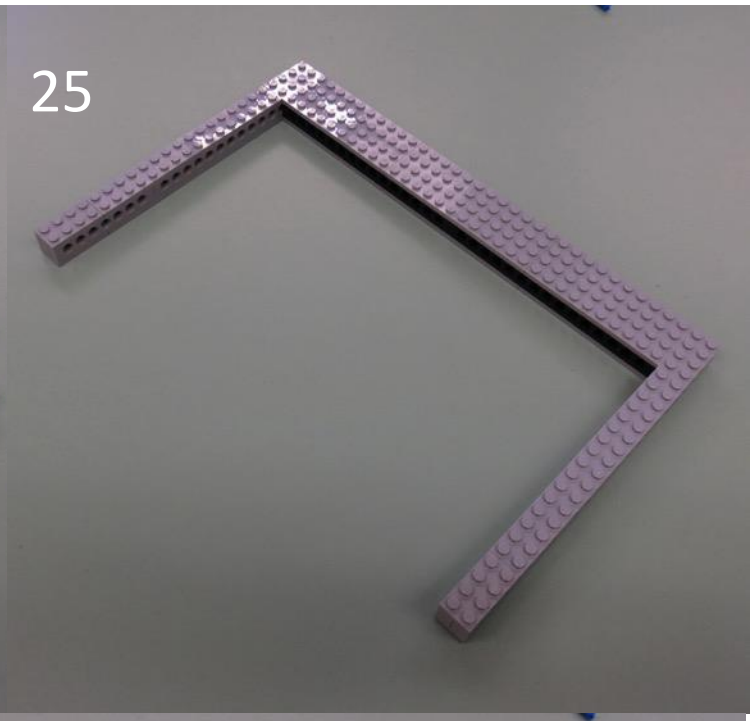

24

Pieces needed:

4x12 gray plate (x3)

25

Assemble pieces from steps 18-24 to make laser arm

26

Pieces needed:

Thorlabs polarizer

Screws to mount polarizer (x2)

Gray connectors (x2)

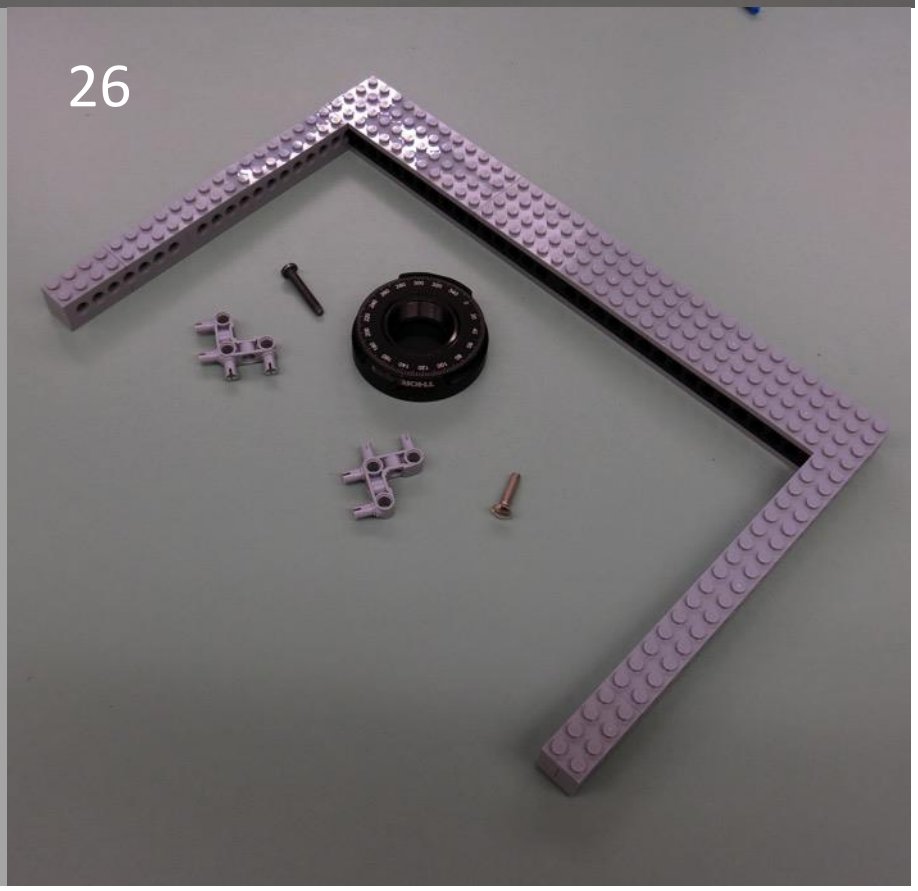

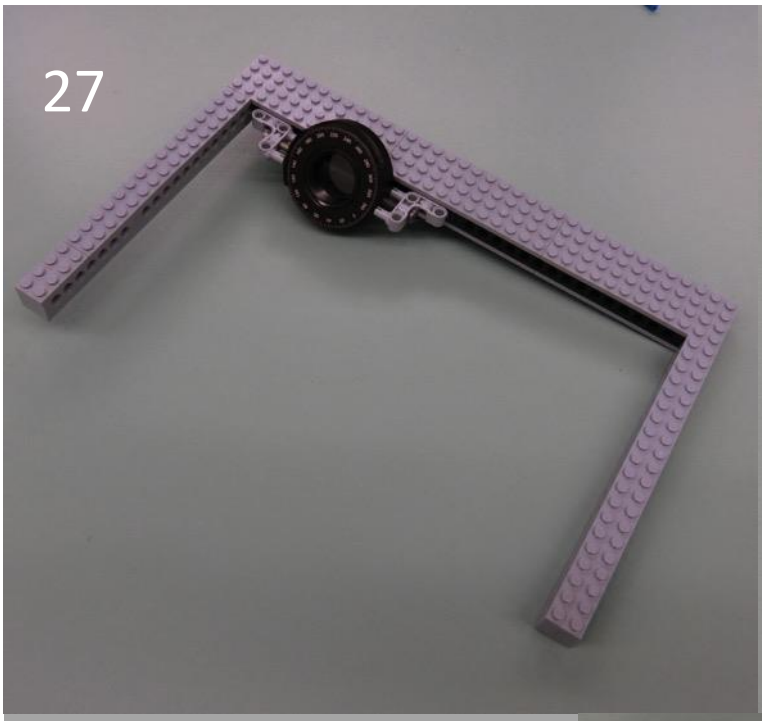

27 Click polarizer into laser arm in position desired

28 Pieces needed:

2x8 gray plate with holes

Laser (many devices are compatible with Lego brick spacing, but screw holes can be drilled through plastic as needed.)

29 Pieces needed:

3 long blue connectors (x4)

2x8 gray plate with holes

30 Click laser into laser arm in position desired

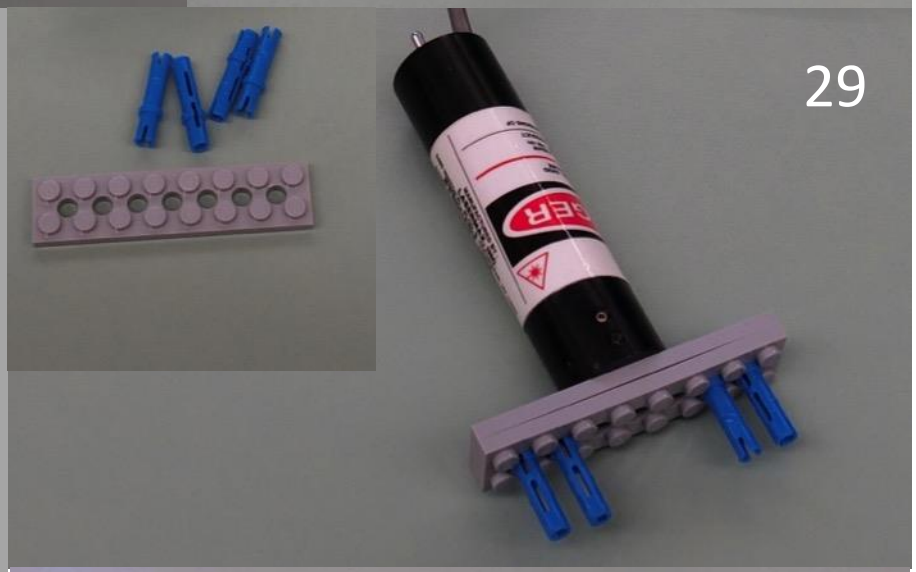

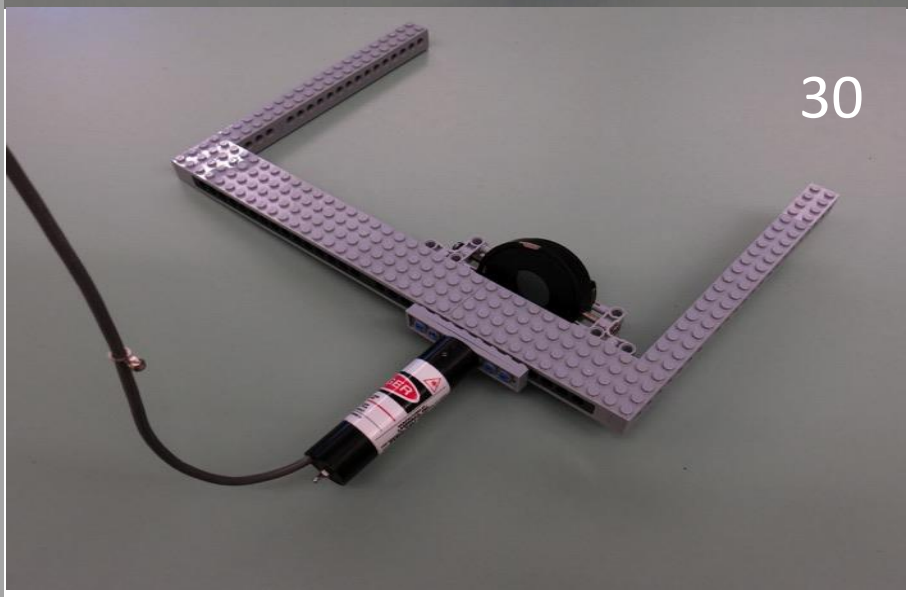

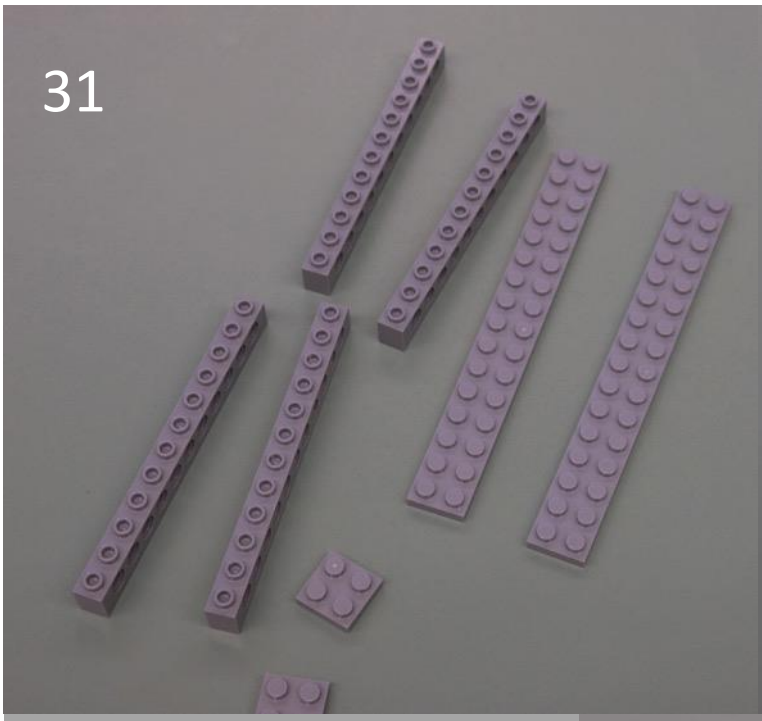

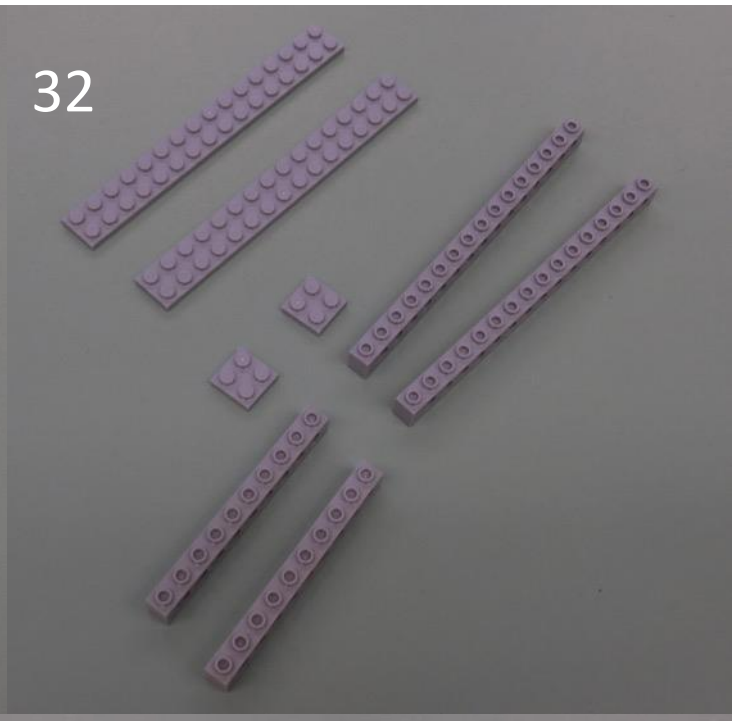

31

Pieces needed:

2x16 gray plates (x2)

2x2 gray plates (x2)

12 long gray technic bricks (x4)

32

Pieces needed:

2x16 gray plates (x2)

2x2 gray plates (x2)

16 long gray technic bricks (x2)

10 long gray technic bricks

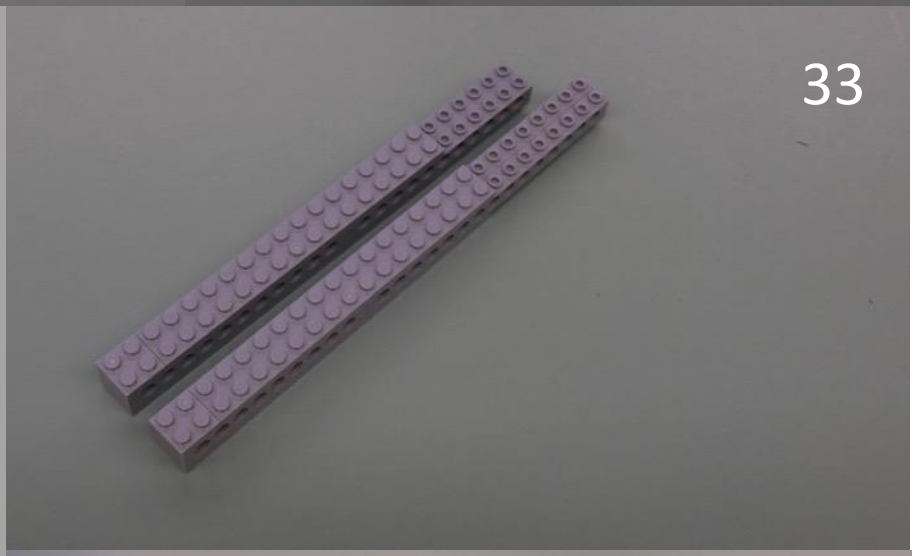

33

Put together pieces from steps 31-32 into arms

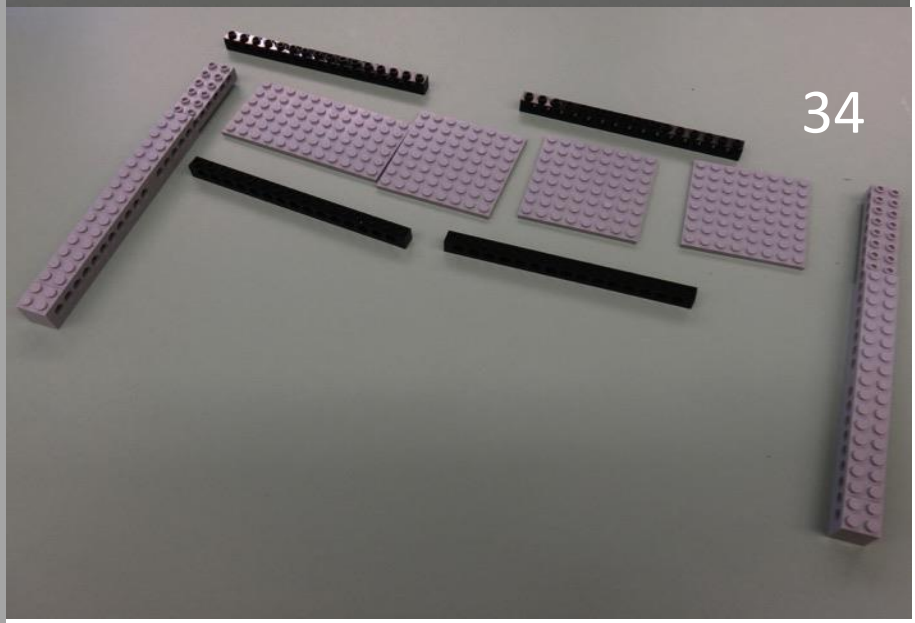

34

Pieces needed:

6x12 gray plate

8x8 gray plate (x3)

16 long black technic brick (x4)

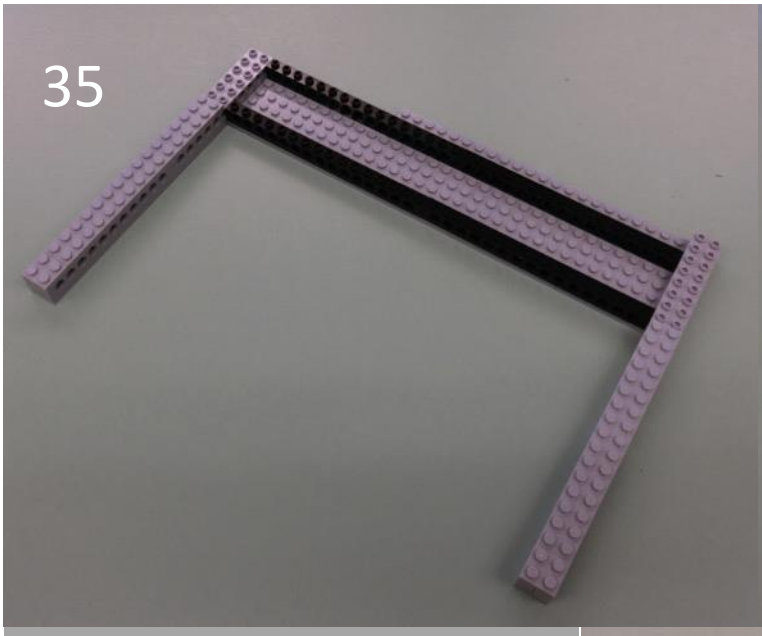

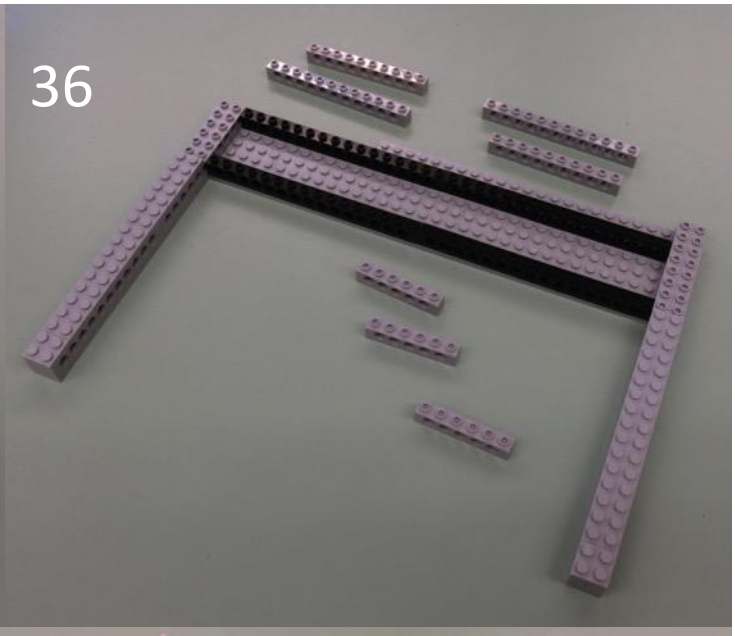

35 Assemble arms from steps 31-33 and pieces from 34 together as shown

36 Pieces needed:

10 long gray technic brick (x2)

12 long gray technic brick (x2)

6 long gray technic bricks (x3)

10 long gray technic bricks (x2)

37 Assemble bricks from step 36 as shown.

Pieces needed:

6x12 gray plate

8x8 gray plate

2x8 gray plate

38 Pieces needed:

Mindstorm motor

8 long gray technic brick (x2)

16 long gray technic brick

3 long blue connector (x2)

2 long black connector (x2)

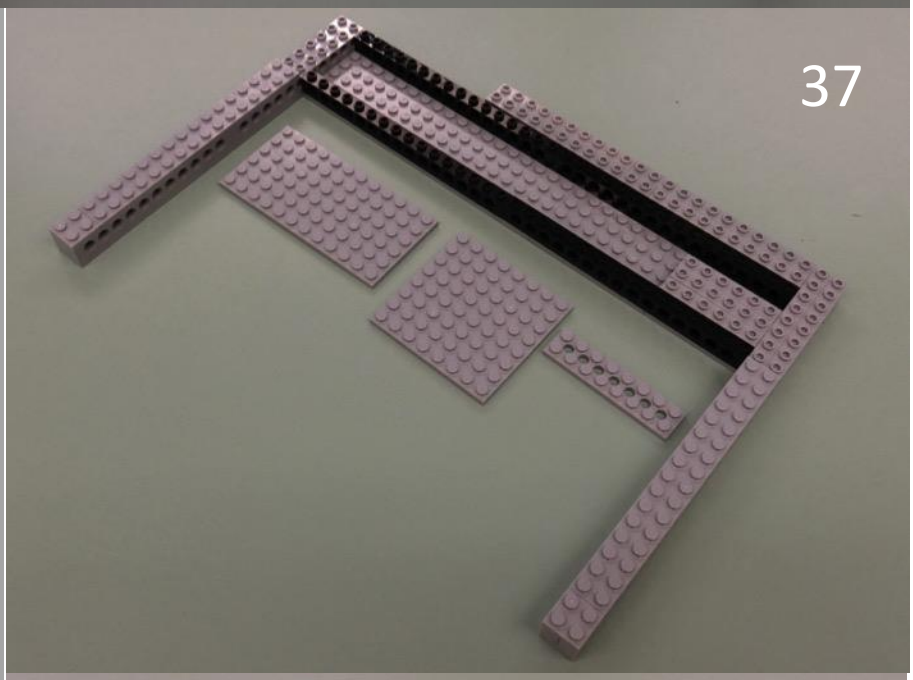

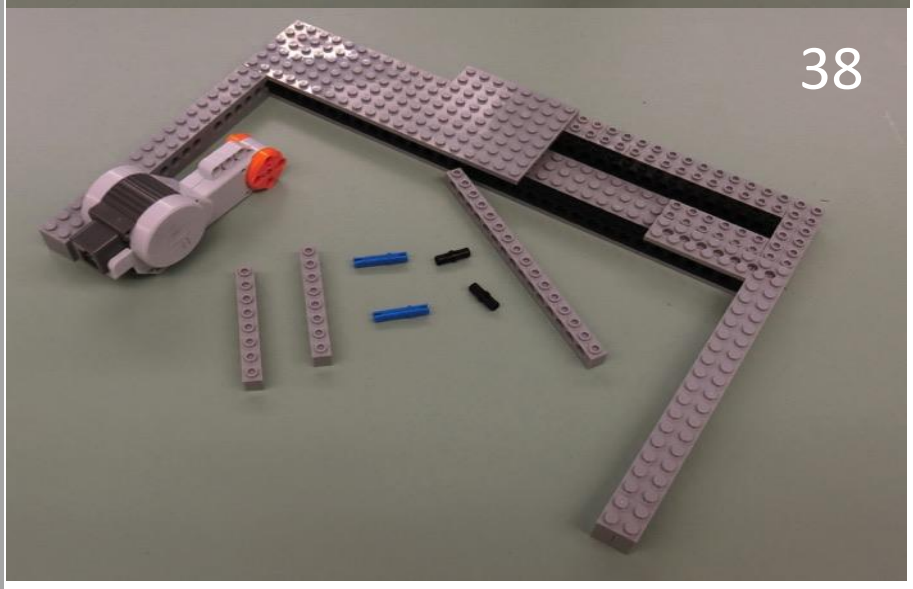

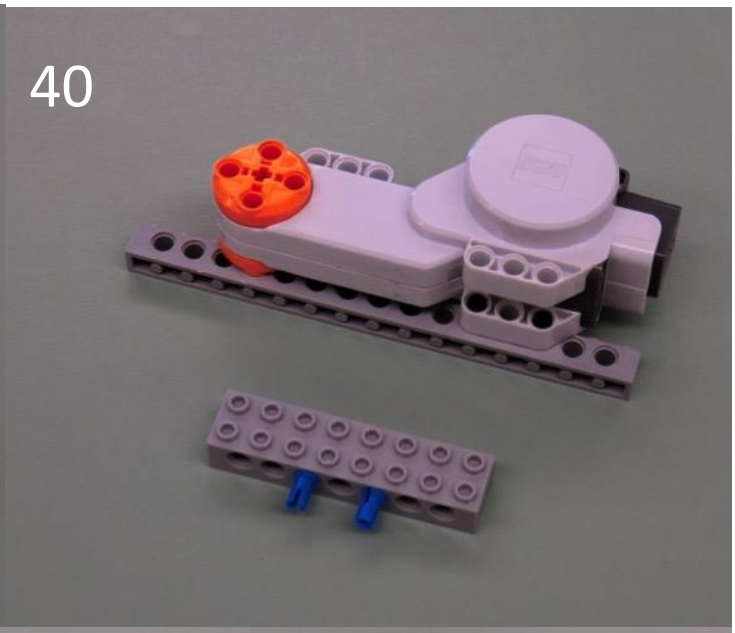

39 Click 16 long brick into motor as shown using pieces from step 38

40 Attach bricks together as shown using pieces from step 38. Click into motor on other side

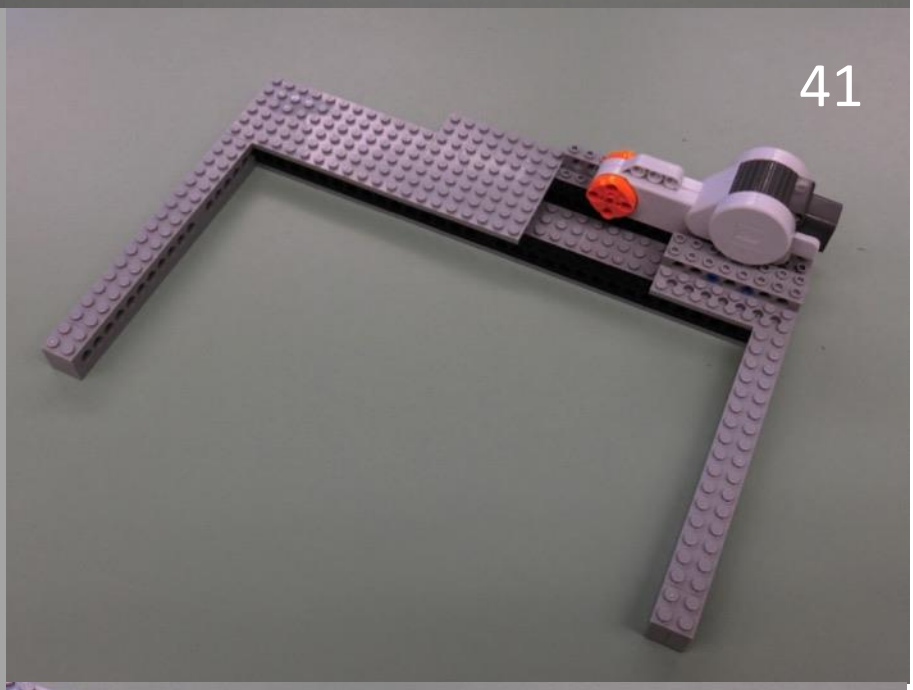

41 Click motor into arm as shown

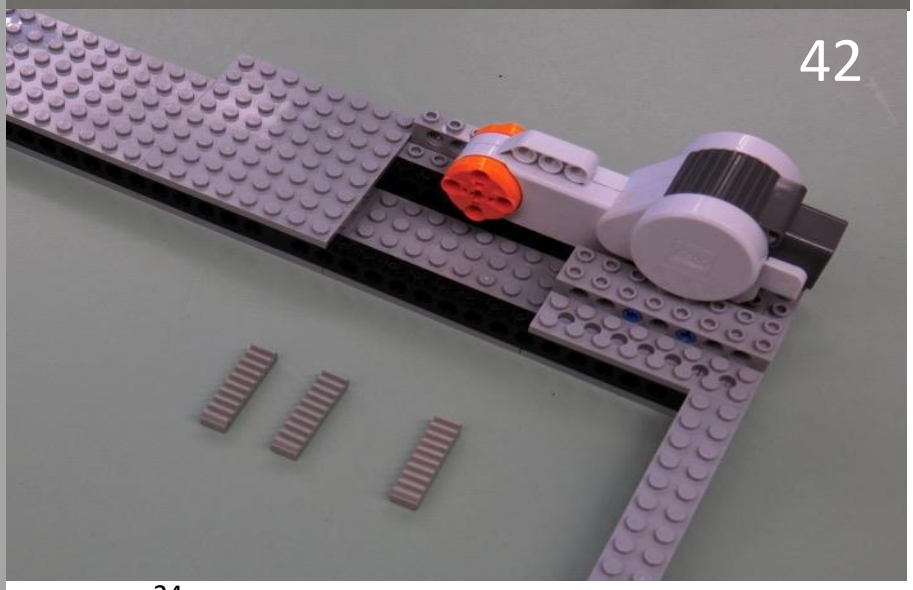

42 Pieces needed:

Flat gray teeth (x3)

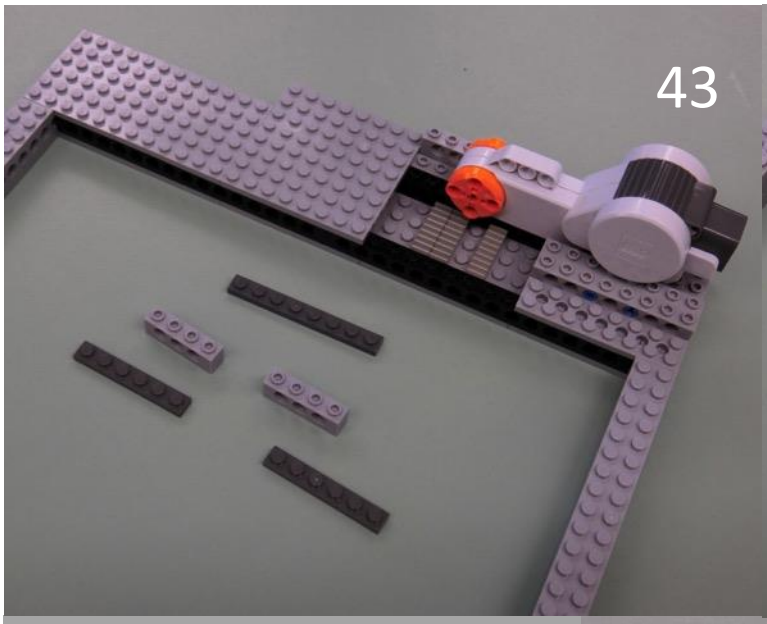

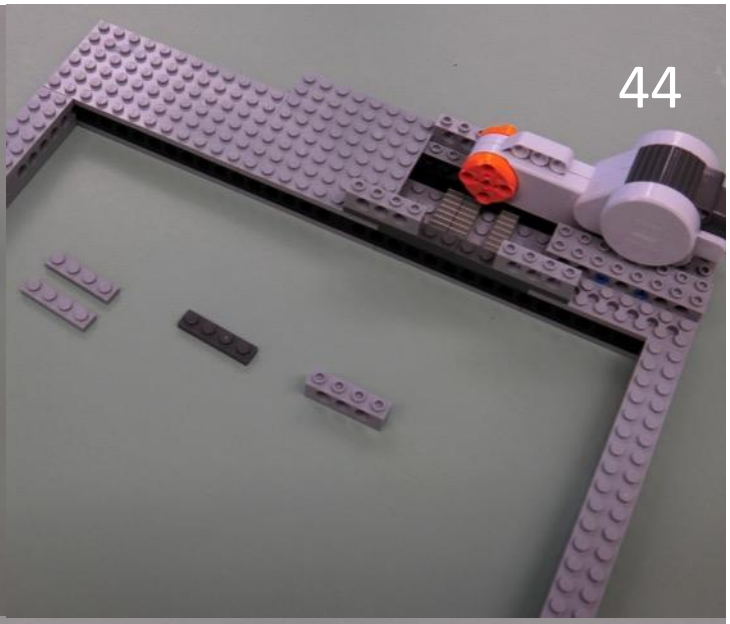

43

Pieces needed:

1x8 long dark gray plate

1x6 long gray plate (x2)

4 long gray technic brick (x2)

44

Pieces needed:

1x4 gray plate (x2)

1x4 dark gray plate

4 long gray technic brick

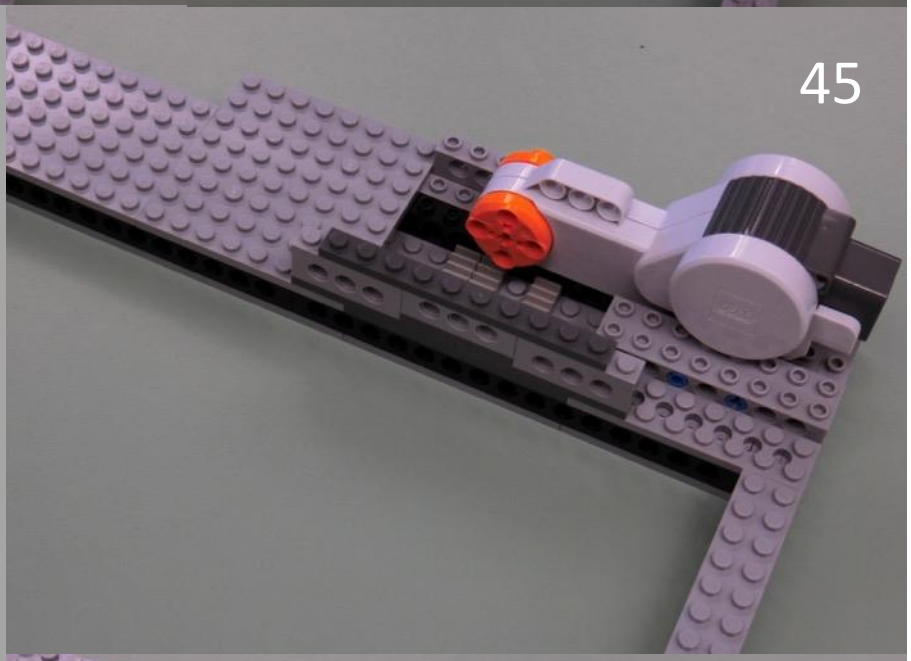

45

Pieces needed:

1x10 dark gray plate

Click in pieces from step 44
and add 1x10 plate on top

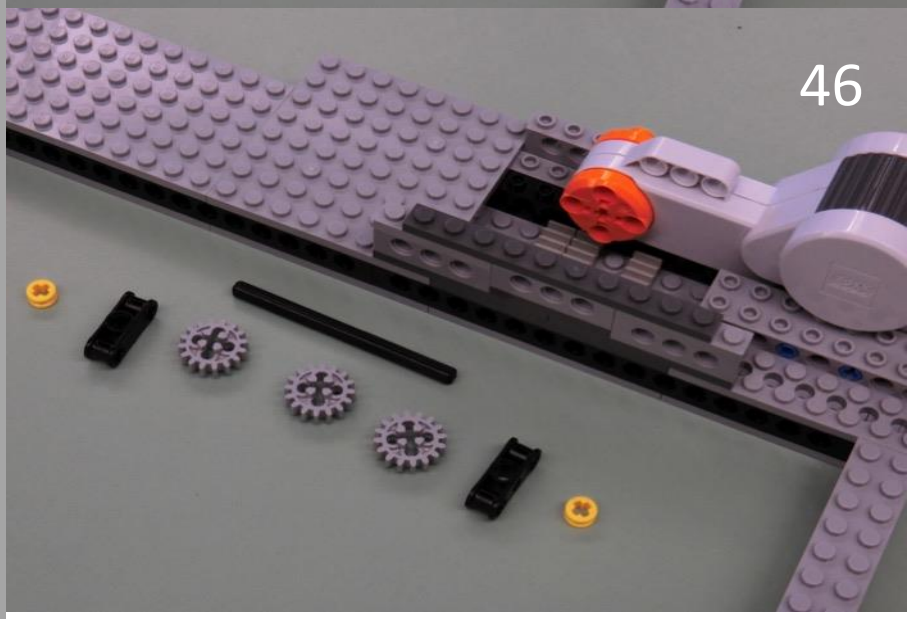

46

Pieces needed:

Small yellow nut (x2)

Black double connecotor (x2)

16 teeth gear (x3)

8 long black rod

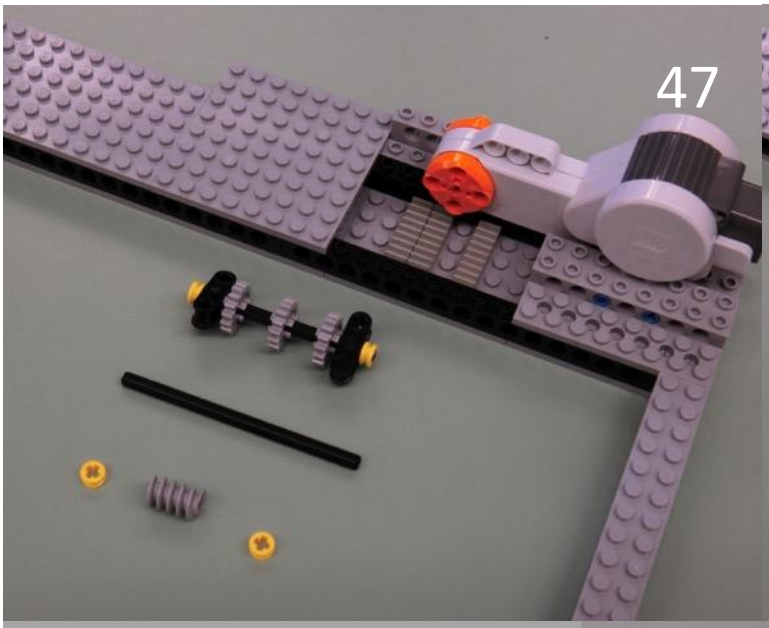

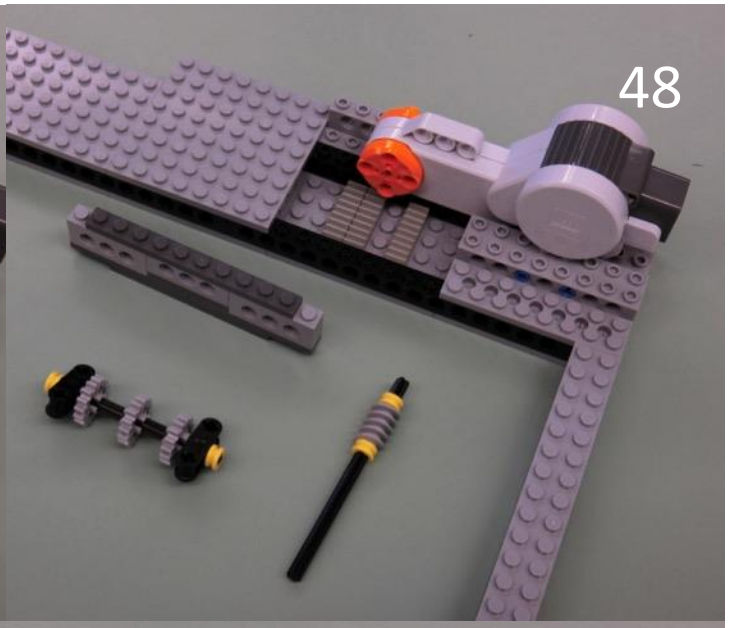

47

Pieces needed:

10 long black rod

small yellow nut (x2)

worm gear

48

Assemble gears as shown an detach bricks from arm for easier installation

49

Insert 3 gear assembly onto flat gray teeth. Insert worm gear assembly into motor such that it interfaces with the middle gear from 3 gear assembly. This motor will turn worm gear and move 3 gear assembly.

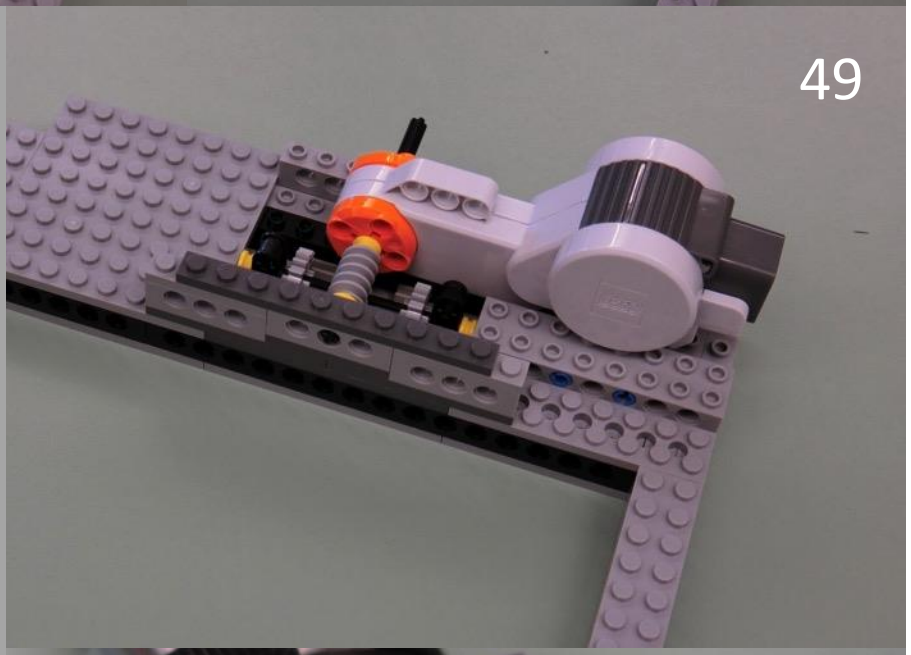

50

Pieces needed:

Point Gray Firewire camera Flea3 FL3-FW-14S3C (or other similar small camera)

2x4 dark gray plate drilled to mount onto top of camera using small screws

gray direction change connector (x2)

Direction change connectors are mounted to camera using hex screws. Connectors were filed down in order to fit Firewire cable into camera. Camera mounting detailed below

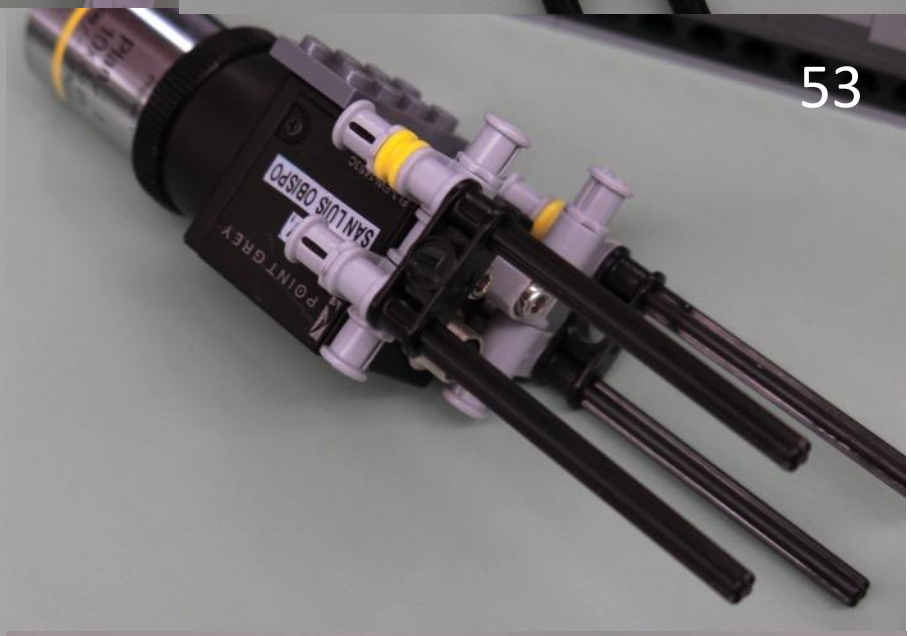

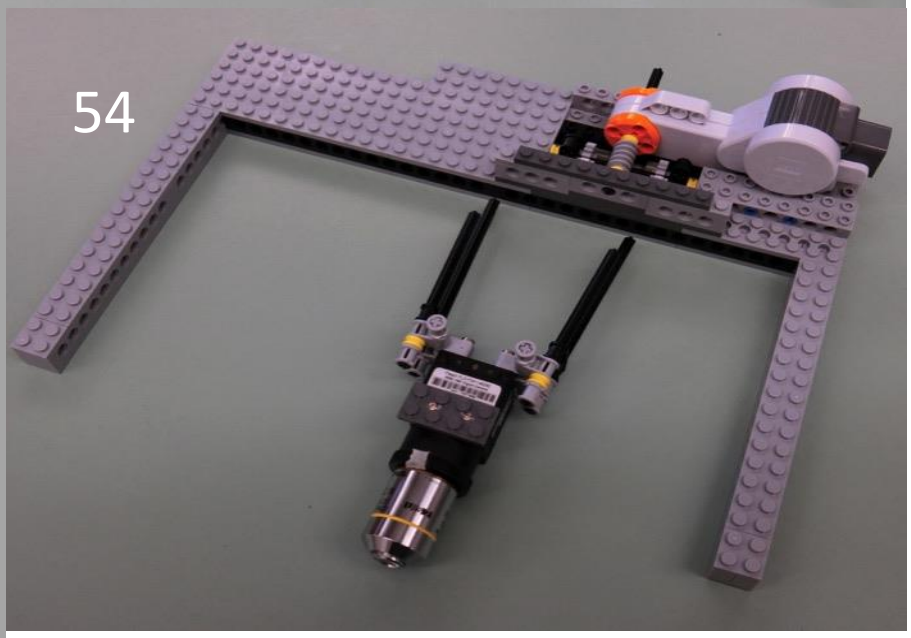

51

Pieces needed:

Small yellow nut

Gray nut (x4)

10 long black rod (x2)

6 long gray rod

Black double connector

Gray direction change connector (x2)

52

Use gray 6 long rod to attach direction change connectors to camera.

53

Use remaining parts from step 51 to attach 10 long black rods to camera assembly. Then repeat steps 51-53 to build second half of camera assembly.

54

Set up entire camera assembly to be inserted into camera arm.

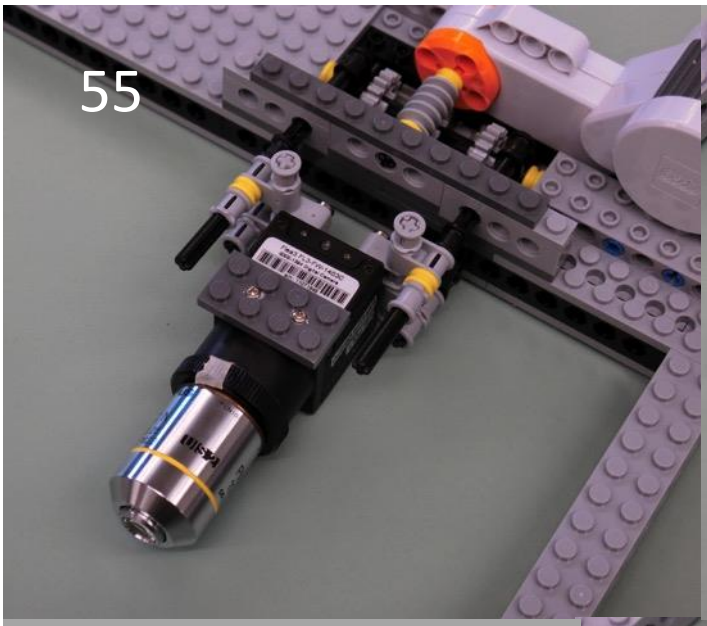

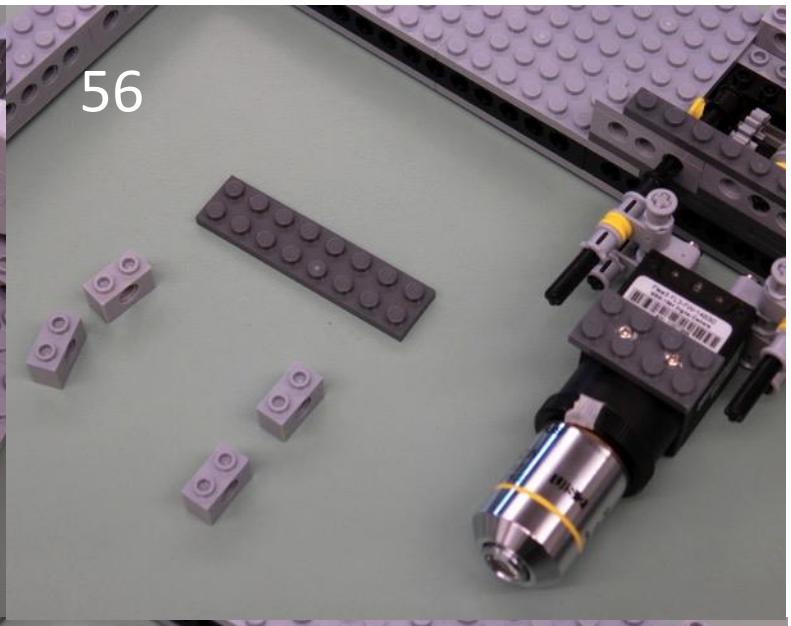

55 Insert camera assembly (steps 50-56) into camera arm (steps 31-49) as shown. Bottom 2 black rods should be flush with gray nuts on camera assembly and should protrude out the back of the technic bricks in the camera arm.

56 Pieces needed:

2 long technic brick (x4)

2x8 dark gray plate

57 Assemble pieces from step 56 as shown.

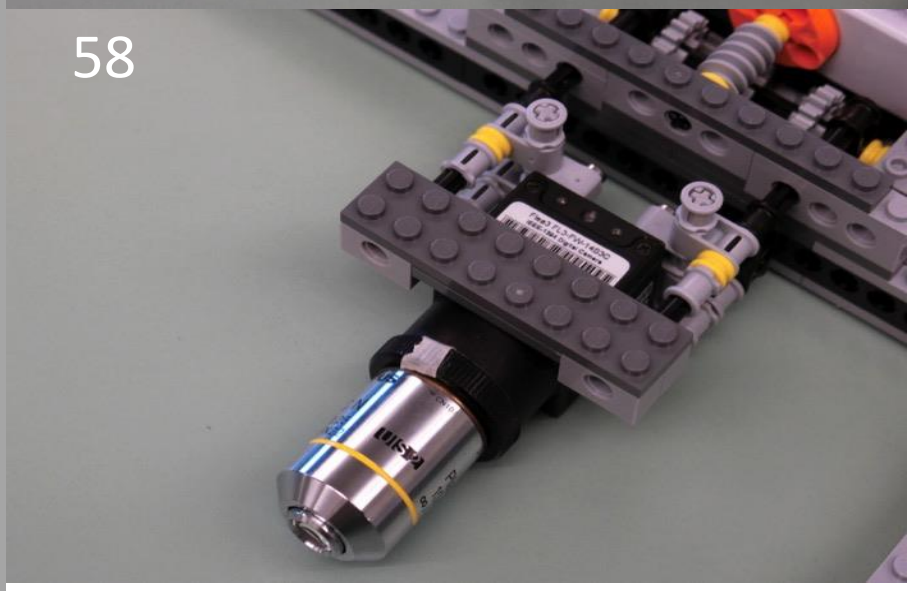

58 Slide bricks from step 57 through black rods on top of camera assembly and click into 2x4 gray plate screwed into camera to stabilize camera.

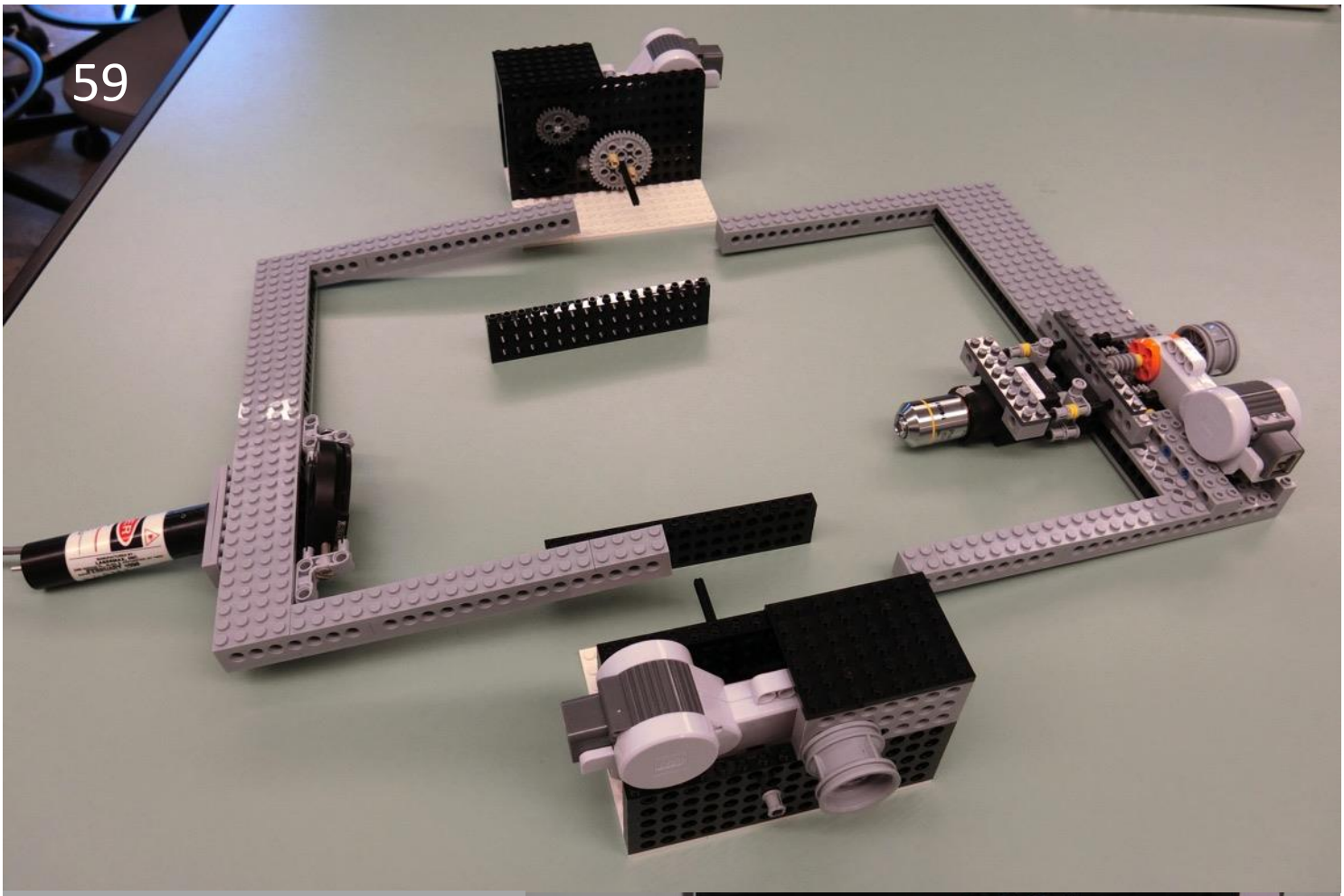

59 Assemble all parts from previous steps as shown. Remove stack of three black technic bricks from motor assemblies as shown.

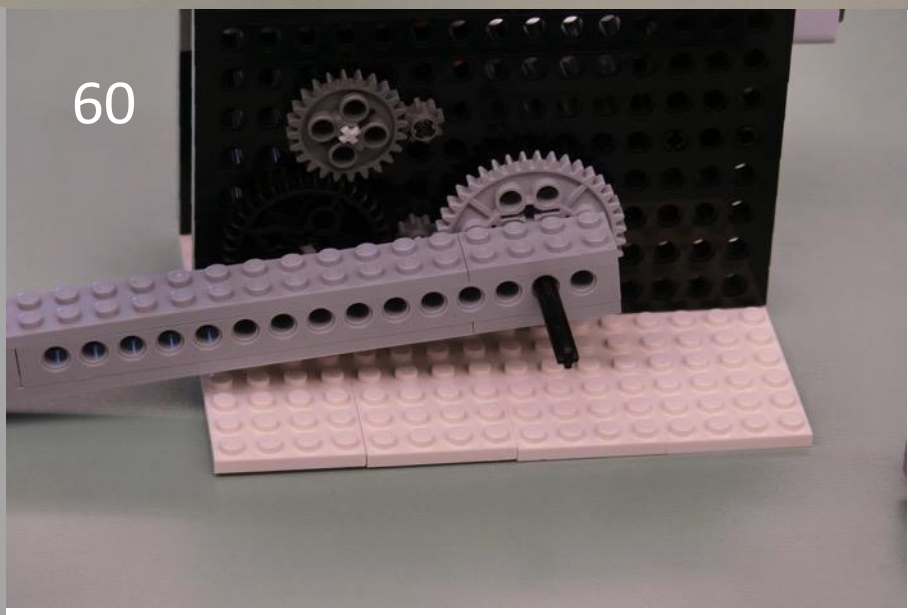

60 Insert black rod into 2nd hole of laser arm and click arm into large gear using 2 tan connectors. Do the same for 2nd motor assembly and the camera arm.

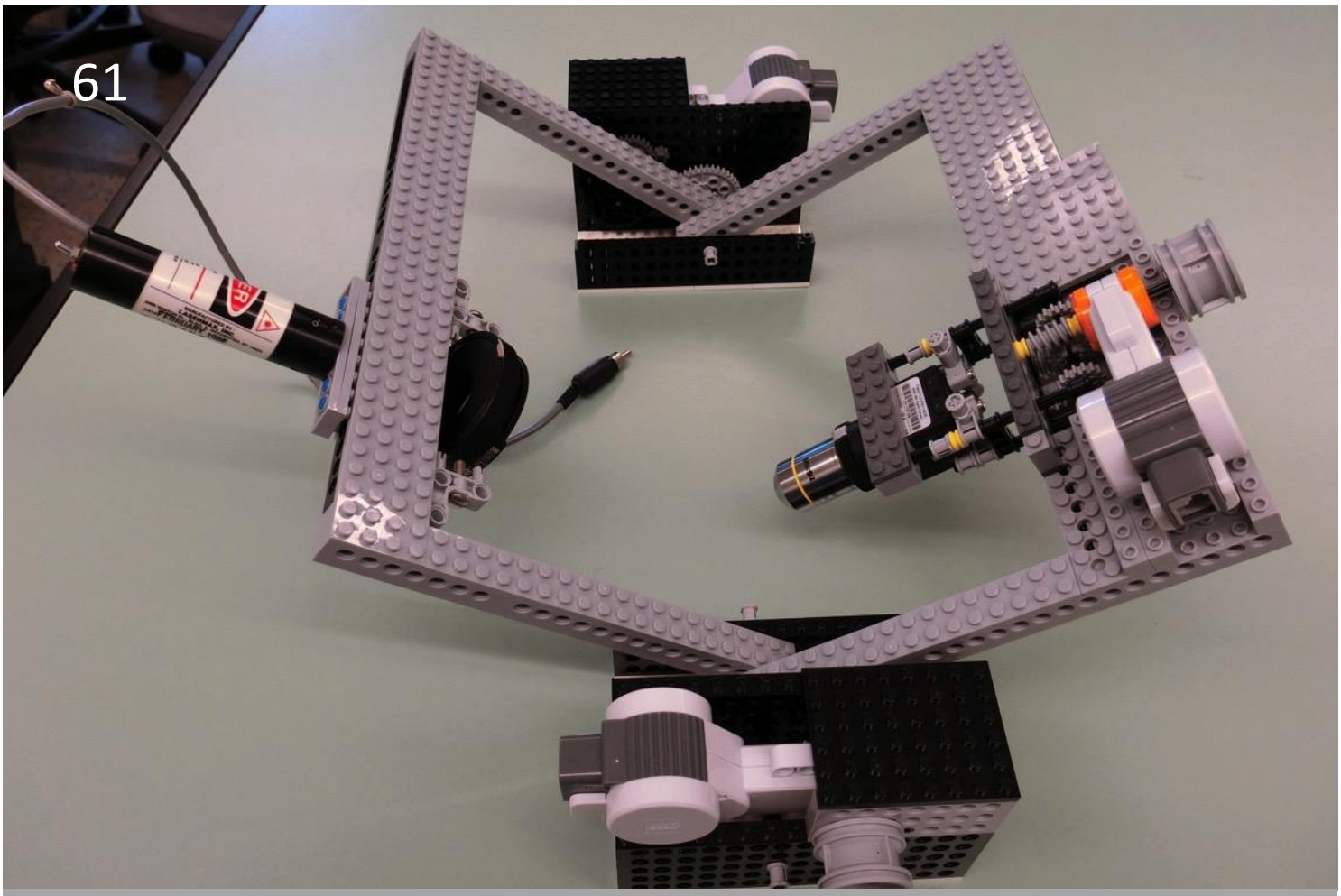

61

Pieces needed:

Grey nut (x2)

Slide both arms and arm motors together so the black rod passes through the 2nd hole from the end of each arm. These 2 rods serve as the main rotation axis of the laser and camera arms.

Click the 3 black technic bricks previously removed in step 59 back to their original positions with the main axis passing through the top brick. Slide gray nut onto black rod to hold axis in place as shown.

Manually rotate arms to approximate position shown using manual rotation wheel on far sides of motor arms.

Hook up your camera to a computer and download necessary software to see image. You can use LabView software found on http://www.calpoly.edu/~jfernsle/ to control arm angles and camera focusing. Your Lego BAM is ready to be adjusted to the Brewster angle and start imaging!